



Probing the nature of the $\chi_{c1}(3872)$ state using radiative decays

LHCb collaboration[†]

Abstract

The radiative decays $\chi_{c1}(3872) \rightarrow \psi(2S)\gamma$ and $\chi_{c1}(3872) \rightarrow J/\psi\gamma$ are used to probe the nature of the $\chi_{c1}(3872)$ state using proton-proton collision data collected with the LHCb detector, corresponding to an integrated luminosity of 9 fb^{-1} . Using the $B^+ \rightarrow \chi_{c1}(3872)K^+$ decay, the $\chi_{c1}(3872) \rightarrow \psi(2S)\gamma$ process is observed for the first time and the ratio of its partial width to that of the $\chi_{c1}(3872) \rightarrow J/\psi\gamma$ decay is measured to be

$$\frac{\Gamma_{\chi_{c1}(3872) \rightarrow \psi(2S)\gamma}}{\Gamma_{\chi_{c1}(3872) \rightarrow J/\psi\gamma}} = 1.67 \pm 0.21 \pm 0.12 \pm 0.04,$$

where the first uncertainty is statistical, the second systematic and the third is due to the uncertainties on the branching fractions of the $\psi(2S)$ and J/ψ mesons. The measured ratio makes the interpretation of the $\chi_{c1}(3872)$ state as a pure $D^0\bar{D}^{*0} + \bar{D}^0D^{*0}$ molecule questionable and strongly indicates a sizeable compact charmonium or tetraquark component within the $\chi_{c1}(3872)$ state.

Submitted to JHEP

© 2024 CERN for the benefit of the LHCb collaboration. CC BY 4.0 licence.

[†]Authors are listed at the end of this paper.

1 Introduction

Decays of beauty hadrons have proven to be a convenient and fruitful tool in the search and study of charmonium-like states, whose measured properties point to the presence of a $c\bar{c}$ component in their quark content, but forbid them to be associated with any conventional charmonium resonance [1–12]. The first such state, $\chi_{c1}(3872)$, was observed in 2003 by the Belle collaboration in the $J/\psi\pi^+\pi^-$ mass spectrum from $B^+ \rightarrow J/\psi\pi^+\pi^-K^+$ decays [13]. For more than two decades since its discovery, the properties of this state have been intensively studied in e^+e^- collisions by the BaBar [14–21], Belle [22–29], and BESIII [30–35] collaborations; in proton-antiproton collisions by the CDF [36–39] and D0 [40] collaborations; in proton-proton (pp) collisions by the ATLAS [41], CMS [42, 43] and LHCb [44–55] collaborations; in proton-ion collisions by the LHCb collaboration [56]; and in lead-lead collisions by the CMS [57] collaboration.

The closeness of the mass of the $\chi_{c1}(3872)$ state [50, 51] to the $D^0\bar{D}^{*0}$ threshold, its narrow width [35, 50, 51], quantum numbers of $J^{PC} = 1^{++}$ [45, 47] and a large coupling to the $D^0\bar{D}^{*0}$ system [18, 23, 24, 29, 35] provide natural arguments to support the interpretation of the $\chi_{c1}(3872)$ state as a loosely-coupled $D^0\bar{D}^{*0} + \bar{D}^0D^{*0}$ molecular state [58–62], in which the colourless open-charm mesons are spatially well separated. However, the expected production cross-section for such a molecular object in high-energy hadron collisions is too small to explain the observed production of the $\chi_{c1}(3872)$ state [63–66]. In fact, the measured production cross-section, transverse momentum and rapidity spectra of the $\chi_{c1}(3872)$ state are close to those observed for conventional charmonium states [36, 40, 41, 44, 53]. Alternative hypotheses for the nature of the $\chi_{c1}(3872)$ state include a charmonium $\chi_{c1}(2P)$ state [67–70], its virtual companion [71] or its mixture with a hadronic molecule [70, 72]; a hadro-charmonium state [73]; a hybrid meson [74, 75] or a tetraquark [76, 77]. A large isospin violation in $\chi_{c1}(3872)$ decays [54] strongly disfavors the interpretation of the $\chi_{c1}(3872)$ particle as a pure charmonium state.

Experimental studies of the $\chi_{c1}(3872)$ lineshape in the $J/\psi\pi^+\pi^-$ [50] and $D^0\bar{D}^{*0}$ [29] final states, and the combined analysis of the two final states [35] provide important information about the parameters of the low-energy $D^0\bar{D}^{*0}$ scattering amplitude, namely the scattering length and the effective range. These parameters, if measured precisely, provide crucial information about the internal structure of the $\chi_{c1}(3872)$ state. The sign of the scattering length, the values of the effective range, and the compositeness parameter [78] indicate the presence of a compact component in the wave function of the $\chi_{c1}(3872)$ state [79, 80]. However, the current experimental precision of these parameters is insufficient for drawing a definite conclusion about the nature of the $\chi_{c1}(3872)$ state. In the future, the precision could potentially be improved with increased data sample size, better mass resolution and, as pointed out in Ref. [29], with a combined analysis of the datasets accumulated by the Belle, Belle II, BESIII and LHCb experiments.

The study of the radiative decays of the $\chi_{c1}(3872)$ state into the $\psi(2S)\gamma$ and $J/\psi\gamma$ final states provides an alternative way to probe its nature [81]. Calculations for the ratio of the partial radiative decay widths into $\psi(2S)\gamma$ and $J/\psi\gamma$ final states,

$$\mathcal{R}_{\psi\gamma} \equiv \frac{\Gamma_{\chi_{c1}(3872) \rightarrow \psi(2S)\gamma}}{\Gamma_{\chi_{c1}(3872) \rightarrow J/\psi\gamma}}, \quad (1)$$

vary widely depending on the hypothesis considered for the nature of the $\chi_{c1}(3872)$ state. Each partial radiative width is subject to a sizeable theoretical uncertainty, while a signif-

Table 1: Compilation of predictions for the ratio $\mathcal{R}_{\psi\gamma}$ of radiative partial decay widths of the $\chi_{c1}(3872)$ state. The last column indicatively marks the considered model: $c\bar{c}$ for predominantly charmonium $\chi_{c1}(2P)$ models; $c\bar{c}/vc$ for the model of a virtual companion of the $\chi_{c1}(2P)$ state; $D\bar{D}^*$ for the predominantly $D^0\bar{D}^{*0} + \bar{D}^0D^{*0}$ molecular model and models where the molecular component is mixed with $J/\psi\rho$ and/or $J/\psi\omega$ components and a compact component; and $c\bar{c}q\bar{q}$ for the compact tetraquark model. The value of $\mathcal{R}_{\psi\gamma}$ from Ref. [82] is expressed in terms of the poorly known ratio of the coupling constants, (g'_2/g_2) , for the $\psi(2S)$ and J/ψ mesons with $\bar{D}^{(*)}D^{(*)}$ systems, which are expected to be similar. The same ratio of coupling constants dictates the wide spread of predictions from Ref. [83]. The value in the last row is the minimal possible value of the ratio $\mathcal{R}_{\psi\gamma}$ in this model; the ratio can be as big as 12 for large diquark sizes.

| Reference | | $\mathcal{R}_{\psi\gamma}$ | |
|--|------|----------------------------|--------------------|
| T. Barnes and S. Godfrey | [67] | 5.8 | $c\bar{c}$ |
| T. Barnes, S. Godfrey and S. Swanson | [69] | 2.6 | $c\bar{c}$ |
| F. De Fazio | [84] | (1.64 ± 0.25) | $c\bar{c}$ |
| B.-Q. Li and K. T. Chao | [85] | 1.3 | $c\bar{c}$ |
| Y. Dong <i>et al.</i> | [86] | 1.3 – 5.8 | $c\bar{c}$ |
| A. M. Badalian <i>et al.</i> | [87] | (0.8 ± 0.2) | $c\bar{c}$ |
| J. Ferretti, G. Galata and E. Santopinto | [88] | 6.4 | $c\bar{c}$ |
| A. M. Badalian, Yu. A. Simonov and B. L. G. Bakker | [89] | 2.4 | $c\bar{c}$ |
| W. J. Deng <i>et al.</i> | [90] | 1.3 | $c\bar{c}$ |
| F. Giacosa, M. Piotrowska and S. Goito | [71] | 5.4 | $c\bar{c}/vc$ |
| E. S. Swanson | [81] | 0.38 % | $D\bar{D}^*$ |
| Y. Dong <i>et al.</i> | [86] | 0.33 % | $D\bar{D}^*$ |
| D. P. Rathaud and A. K. Rai | [91] | 0.25 | $D\bar{D}^*$ |
| R. F. Lebed and S. R. Martinez | [92] | 0.33 % | $D\bar{D}^*$ |
| B. Grinstein, L. Maiani and A. D. Polosa | [93] | 3.6 % | $D\bar{D}^*$ |
| F.-K. Guo <i>et al.</i> | [82] | $0.21(g'_2/g_2)^2$ | $D\bar{D}^*$ |
| D. A.-S. Molnar, R. F. Luiz and R. Higa | [83] | 2 – 10 | $D\bar{D}^*$ |
| E. Cincioglu <i>et al.</i> | [94] | < 4 | $D\bar{D}^*$ |
| S. Takeuchi, M. Takizawa and K. Shimizu | [95] | 1.1 – 3.4 | $D\bar{D}^*$ |
| B. Grinstein, L. Maiani and A. D. Polosa | [93] | $> (0.95^{+0.01}_{-0.07})$ | $c\bar{c}q\bar{q}$ |

icant part of this uncertainty cancels in the ratio of decay widths. The theoretical predictions for the ratio $\mathcal{R}_{\psi\gamma}$ for a variety of the considered models are summarised in Table 1. As a general rule, large values of this ratio, $\mathcal{R}_{\psi\gamma} \gtrsim 1$, are expected under the assumption that the $\chi_{c1}(3872)$ state is a conventional charmonium $\chi_{c1}(2P)$ state [67, 69, 71, 84–90], while calculations based on the pure $D\bar{D}^*$ -molecular hypothesis give much smaller values, $\mathcal{R}_{\psi\gamma} \ll 1$ [81, 86, 91–93], unless specific assumptions on the poorly known ratio of the coupling constants (g'_2/g_2) for the $\psi(2S)$ and J/ψ mesons with $\bar{D}^{(*)}D^{(*)}$ systems [82, 83] are used. Models based on the mixture of a predominantly $D\bar{D}^*$ molecular state (and sometimes also with $J/\psi\rho$ and $J/\psi\omega$ contributions) and a compact component cover a wide range of $\mathcal{R}_{\psi\gamma}$, but they have reduced predictive power due to their large dependency on the mixing parameters [94, 95]. The first calculations based on the Born–Oppenheimer approximation for the $c\bar{c}q\bar{q}$ tetraquark [93] give a result that is similar to expectations

from the charmonium models.

Experimentally, the BaBar collaboration reported the first evidence of the $\chi_{c1}(3872) \rightarrow \psi(2S)\gamma$ decay and measured $\mathcal{R}_{\psi\gamma} = 3.4 \pm 1.4$ [20]. Subsequently, evidence for the same decay was found by the LHCb experiment using data collected in pp collisions in 2011-2012 at center-of-mass energies of 7 and 8 TeV, corresponding to an integrated luminosity of 3 fb^{-1} [46]. The measured $\mathcal{R}_{\psi\gamma}$ value of $2.46 \pm 0.64 \pm 0.29$ is in good agreement with the value obtained by the BaBar collaboration. On the other hand, the Belle [26] and BESIII [32] collaborations did not observe significant signals of the $\chi_{c1}(3872) \rightarrow \psi(2S)\gamma$ decay. The most stringent upper limit is set by the BESIII collaboration, $\mathcal{R}_{\psi\gamma} < 0.59$ (at 90% CL), and is in tension with the values reported by the BaBar and LHCb collaborations.

This paper reports a study of the radiative decays of the $\chi_{c1}(3872)$ state into the $\psi(2S)\gamma$ and $J/\psi\gamma$ final states using the $B^+ \rightarrow \chi_{c1}(3872)K^+$ decay. The ratio of decay widths $\mathcal{R}_{\psi\gamma}$ defined in Eq. (1) is measured as the ratio of branching fractions for the $B^+ \rightarrow (\chi_{c1}(3872) \rightarrow \psi\gamma)K^+$ decays,¹

$$\mathcal{R}_{\psi\gamma} = \frac{\mathcal{B}_{B^+ \rightarrow (\chi_{c1}(3872) \rightarrow \psi(2S)\gamma)K^+}}{\mathcal{B}_{B^+ \rightarrow (\chi_{c1}(3872) \rightarrow J/\psi\gamma)K^+}}. \quad (2)$$

The analysis is based on pp collision data collected with the LHCb detector for two data-taking periods, Run 1 and Run 2. The first sample was previously analysed in Ref. [46]. The second sample was collected between 2015 and 2018 at a centre-of-mass energy of 13 TeV and corresponds to an integrated luminosity of 6 fb^{-1} .

2 Detector and simulation

The LHCb detector [96, 97] is a single-arm forward spectrometer covering the pseudorapidity range $2 < \eta < 5$, designed for the study of particles containing b or c quarks. The detector includes a high-precision tracking system consisting of a silicon-strip vertex detector surrounding the pp interaction region [98], a large-area silicon-strip detector located upstream of a dipole magnet with a bending power of about 4 T m, and three stations of silicon-strip detectors and straw drift tubes [99, 100] placed downstream of the magnet. The tracking system provides a measurement of the momentum, p , of charged particles with a relative uncertainty that varies from 0.5% at low momentum to 1.0% at 200 GeV/c. The minimum distance of a track to a primary pp collision vertex (PV), the impact parameter, is measured with a resolution of $(15 + 29/p_T) \mu\text{m}$, where p_T is the component of the momentum transverse to the beam, in GeV/c. Different types of charged hadrons are distinguished using information from two ring-imaging Cherenkov detectors [101]. Photons, electrons and hadrons are identified by a calorimeter system consisting of scintillating-pad and preshower detectors, an electromagnetic and a hadronic calorimeter. Muons are identified by a system composed of alternating layers of iron and multiwire proportional chambers [102].

The online event selection is performed by a trigger [103, 104], which consists of a hardware stage, based on information from the calorimeter and muon systems, followed by a software stage, which applies a full event reconstruction. At the hardware trigger

¹In this paper inclusion of charge-conjugate decays is implied throughout, and the symbol ψ denotes the J/ψ and $\psi(2S)$ states together.

stage, events are required to have a muon track with high transverse momentum or dimuon candidates in which the product of the p_T of the muons has a high value. In the software trigger, two oppositely charged muons are required to form a good-quality vertex that is significantly displaced from any PV, with a dimuon mass exceeding $2.7 \text{ GeV}/c^2$.

Simulated events are used to describe signal shapes, background from partially reconstructed decays of beauty hadrons, and to compute the efficiencies needed to determine the ratio $\mathcal{R}_{\psi\gamma}$. In the simulation, pp collisions are generated using PYTHIA [105] with a specific LHCb configuration [106]. Decays of unstable particles are described by EVTGEN [107], in which final-state radiation is generated using PHOTOS [108]. The interaction of the generated particles with the detector, and its response, are implemented using the GEANT4 toolkit [109, 110] as described in Ref. [111]. The p_T and rapidity (y) spectra of the B^+ mesons in simulation are corrected to match data. The correction factors are calculated by comparing the observed p_T and y spectra for a high-purity sample of reconstructed $B^+ \rightarrow J/\psi K^+$ decays with the corresponding simulated samples. In simulation, the variables used for the kaon identification are resampled according to the calibration data samples of $D^{*+} \rightarrow (D^0 \rightarrow K^- \pi^+) \pi^+$ decays [112]. The procedure accounts for the dependence of the kaon identification on the particle p_T and η as well as the charged particle multiplicity in the event. The track multiplicity for simulated events is corrected to match that in the $B^+ \rightarrow J/\psi K^+$ data sample. The track reconstruction efficiency is corrected using a sample of $J/\psi \rightarrow \mu^+ \mu^-$ decays in data [113], to account for imperfections in the simulation. Samples of $B^+ \rightarrow J/\psi (K^{*+} \rightarrow K^+ \pi^0)$ decays with $\pi^0 \rightarrow \gamma\gamma$ are used to correct the photon reconstruction efficiency in the simulation [114–118].

Large simulated samples of inclusive B meson decays to final states with a charmonium, $B \rightarrow \psi X$, are used to study the background contributions from partially reconstructed decays. The $B^+ \rightarrow J/\psi K^{*+}$ decay with $K^{*+} \rightarrow K^+ \pi^0$, and inclusive $B \rightarrow \psi(2S) K^+ X$ decays, are the most important contributions to the background. An amplitude model determined from $B^0 \rightarrow J/\psi K^{*0}$ decays [119] is used to produce the simulated sample of $B^+ \rightarrow J/\psi (K^{*+} \rightarrow K^+ \pi^0)$ decays. The simulated sample of $B \rightarrow \psi(2S) K^+ X$ decays comprises relevant admixture of B^+ and B^0 mesons. For each sample the individual decays of beauty mesons are simulated as an incoherent mixture of the decays via various excited kaons, namely K^* , $K_0^*(700)$, $K_1(1270)$, $K^*(1410)$, $K_2^*(1430)$, $K^*(1680)$; as well as decays into nonresonant $\psi(2S) K^+ \pi$, $\psi(2S) K^+ \pi\pi$, $\psi(2S) K^+ \eta$, $\psi(2S) K^+ \omega$ and $\psi(2S) K^* \eta$ combinations. The relevant branching fractions are taken from Refs. [8, 120–122], inferred from isospin symmetry, or estimated based on similar decays where no other information exists.

3 Event selection

The $B^+ \rightarrow (\chi_{c1}(3872) \rightarrow \psi\gamma) K^+$ decay candidates are reconstructed using the $\psi \rightarrow \mu^+ \mu^-$ decay mode. Signal candidates are reconstructed by first applying a loose initial selection, and subsequently using a multivariate classifier to suppress backgrounds. To reduce systematic uncertainties, the initial selection criteria for both decay modes are kept the same whenever possible and similar to those used in previous LHCb studies [46, 123].

The muon and kaon candidates are identified by combining information from the Cherenkov detectors, calorimeters and muon detectors [124] associated to the reconstructed tracks. To reduce the combinatorial background, only tracks that are inconsistent with originating from any reconstructed PV in the event are considered. The trans-

verse momentum of muon candidates is required to be greater than 550 MeV/c. Pairs of oppositely charged muons consistent with originating from a common vertex are combined to form ψ candidates. The reconstructed mass of the muon pair is required to be $3.020 < m_{\mu^+\mu^-} < 3.125 \text{ GeV}/c^2$ and $3.597 < m_{\mu^+\mu^-} < 3.730 \text{ GeV}/c^2$ for J/ψ and $\psi(2S)$ candidates, respectively,

Charged particles identified as kaons are required to have $p_T > 200 \text{ MeV}/c$. Photons are reconstructed from clusters in the electromagnetic calorimeter not associated with reconstructed tracks [125–127]. Each selected J/ψ and $\psi(2S)$ candidate is combined with a photon to form a $\chi_{c1}(3872)$ candidate. The transverse energy of the photon candidate should exceed 1.0 GeV and 0.5 GeV for the $\chi_{c1}(3872) \rightarrow J/\psi\gamma$ and $\chi_{c1}(3872) \rightarrow \psi(2S)\gamma$ decays, respectively. Finally the B^+ candidate is obtained by combining a kaon and the $\chi_{c1}(3872)$ candidate.

To suppress contributions from $B^+ \rightarrow J/\psi K^+$ and $B^+ \rightarrow \psi(2S)K^+$ decays, ψK^+ combinations with a mass within $\pm 40 \text{ MeV}/c^2$ of the known B^+ mass [120] are rejected. A good quality kinematic fit [128] is required, which constrains the dimuon mass to the known J/ψ or $\psi(2S)$ mass [120] and requires the B^+ candidate to originate from its associated PV. The B^+ decay time is required to exceed $100 \mu\text{m}/c$ to suppress the large combinatorial background from tracks originating from a PV.

A multilayer perceptron (MLP) classifier is applied to candidate events to reduce background further. The classifier is based on an artificial neural network algorithm [129, 130], configured with a cross-entropy cost estimator [131]. Different classifiers are trained separately for the $B^+ \rightarrow (\chi_{c1}(3872) \rightarrow \psi(2S)\gamma) K^+$ and $B^+ \rightarrow (\chi_{c1}(3872) \rightarrow J/\psi\gamma) K^+$ decay modes. Both classifiers use the same input variables. These are related to the reconstruction quality, kinematics and decay time of the B^+ candidates, kinematics of the final-state particles and variables that characterise the kaon and photon identification. The classifiers are trained using simulated samples of $B^+ \rightarrow \chi_{c1}(3872)K^+$ decays as a proxy for the signal, but different types of background samples for the two decay modes. For the $B^+ \rightarrow (\chi_{c1}(3872) \rightarrow J/\psi\gamma) K^+$ sample, the background after the initial selection is large and mainly consists of random combinations of J/ψ and K^+ mesons with a photon. The background training sample is taken from the signal mass sidebands in data, *i.e.* the $B^+ \rightarrow \chi_{c1}(3872)K^+$ candidate decays with the $J/\psi\gamma K^+$ mass outside of the interval $5.25 < m_{J/\psi\gamma K^+} < 5.32 \text{ GeV}/c^2$ and the $J/\psi\gamma$ mass outside of the interval $3.82 < m_{J/\psi\gamma} < 3.93 \text{ GeV}/c^2$. In the $B^+ \rightarrow (\chi_{c1}(3872) \rightarrow \psi(2S)\gamma) K^+$ sample, the combinatorial background is already largely suppressed by the initial loose selection. The remaining background is dominated by contributions from $B \rightarrow \psi(2S)K^+X$ decays. A simulated sample of $B \rightarrow \psi(2S)K^+X$ decays is used as the background proxy for training. To avoid introducing a bias in the MLP evaluation, a k -fold cross-validation technique [132] with $k = 7$ is used in the training of both classifiers.

The requirement on the response of each MLP classifier is chosen to maximise the figure-of-merit $S/\sqrt{B+S}$, where S represents the expected signal yield, and B is the expected background yield. The background yield is calculated from fits to data, while the expected signal yield is estimated as $S = \varepsilon S_0$, where S_0 is the signal yield obtained from a fit to the data with a loose requirement applied, and ε is the relative efficiency of the requirement on the response of the MLP classifier determined from simulation.

The distributions of the $\psi\gamma K^+$ and $\psi\gamma$ masses for the selected B^+ candidates corresponding to the full data sample are shown in Fig. 1. For better visibility the $\psi\gamma K^+$ mass spectra are shown for candidates within the narrow $\psi\gamma$ mass regions around the known

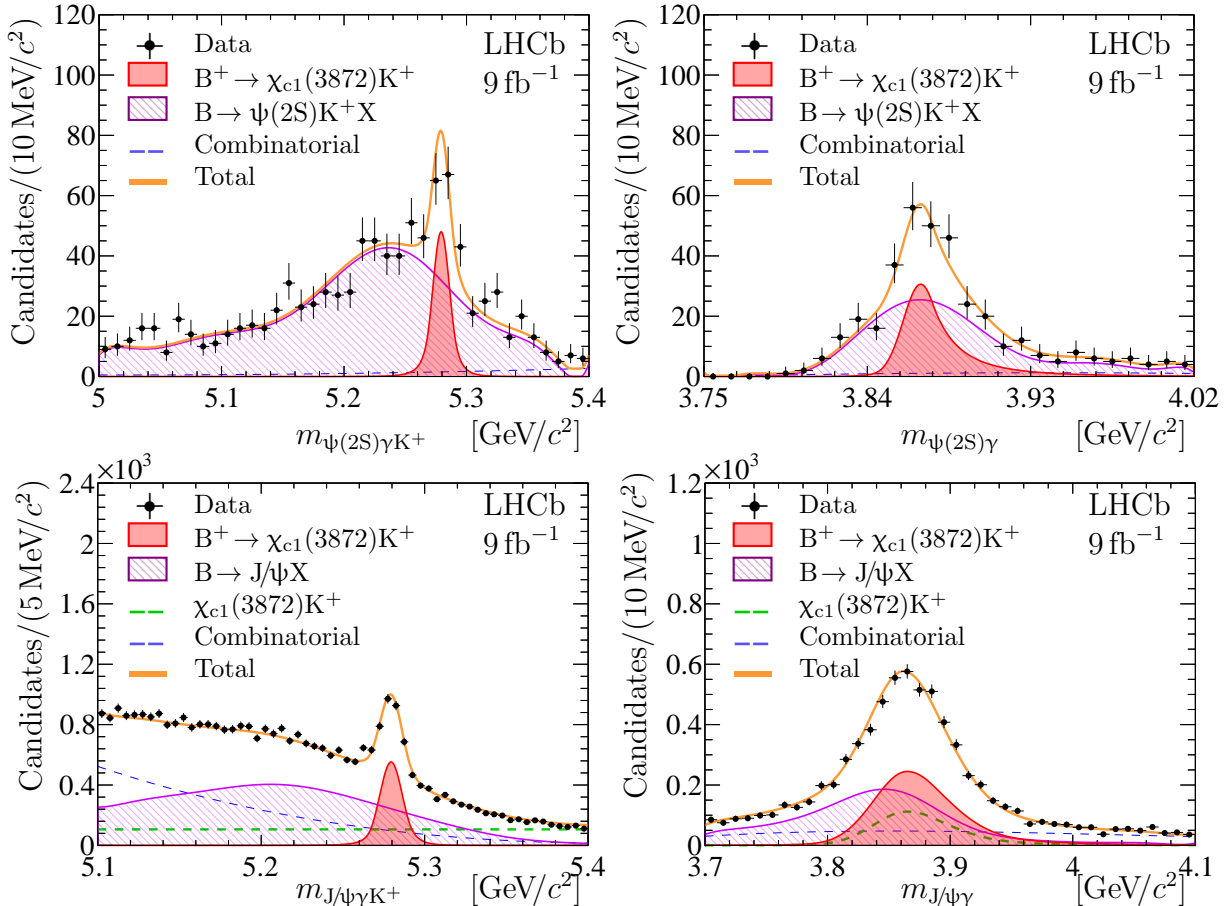


Figure 1: Distributions of the (left) $\psi\gamma K^+$ and (right) $\psi\gamma$ mass of selected B^+ candidates summed over Run1 and Run2 data-taking periods. Top and bottom rows correspond to the $B^+ \rightarrow (\chi_{c1}(3872) \rightarrow \psi(2S)\gamma) K^+$ and $B^+ \rightarrow (\chi_{c1}(3872) \rightarrow J/\psi\gamma) K^+$ candidates, respectively. The $\psi\gamma K^+$ mass spectra are shown for candidates within the narrow $\psi\gamma$ mass regions around the $\chi_{c1}(3872)$ mass, and vice versa, the $\psi\gamma$ mass spectra are shown for candidates within the narrow $\psi\gamma K^+$ mass regions around the B^+ mass. Projections of the fit, described in the text, are overlaid.

$\chi_{c1}(3872)$ mass, $3.842 < m_{\psi(2S)\gamma} < 3.902 \text{ GeV}/c^2$ and $3.782 < m_{J/\psi\gamma} < 3.962 \text{ GeV}/c^2$. Similarly, the $\psi\gamma$ mass spectra are shown for candidates within the narrow $\psi\gamma K^+$ mass regions around the known mass of the B^+ meson, $5.258 < m_{\psi\gamma K^+} < 5.300 \text{ GeV}/c^2$. To improve the mass resolutions the $\psi\gamma K^+$ and $\psi\gamma$ masses are calculated using the kinematic fit described above [128]. In addition, to calculate the $\psi\gamma K^+$ mass, the $\psi\gamma$ mass is constrained to the known value of the $\chi_{c1}(3872)$ state [50, 51, 120]. Clear signals corresponding to both B^+ and $\chi_{c1}(3872)$ states are seen in data for both channels.

4 Signal yield determination

Signal yields of both $B^+ \rightarrow (\chi_{c1}(3872) \rightarrow \psi\gamma) K^+$ decay channels are determined using extended unbinned maximum-likelihood fits to two-dimensional distributions of $m_{\psi\gamma}$ and $m_{\psi\gamma K^+}$. The fit model for the $B^+ \rightarrow (\chi_{c1}(3872) \rightarrow \psi(2S)\gamma) K^+$ decay channel consists

of three components:

1. a signal component parameterised as a product of the B^+ and $\chi_{c1}(3872)$ signal shapes, both described by a modified Gaussian function with power-law tails on both sides of the Gaussian core [133, 134];
2. a background component from the $B \rightarrow \psi(2S)K^+X$ decays, whose shape is determined from the simulation as

$$\sum_{i=0}^n \sum_{j=0}^n \beta_{ij} \mathcal{L}_i(u) \mathcal{L}_j(v), \quad (3a)$$

where u and v stand for the $\psi(2S)\gamma K^+$ and $\psi(2S)\gamma$ masses, reduced to the $-1 \leq u, v \leq 1$ interval, $n = 10$ and $\mathcal{L}_i(u)$ and $\mathcal{L}_j(v)$ are Legendre polynomials. The $(n+1)^2$ coefficients β_{ij} are calculated as

$$\beta_{ij} = \sum_k \frac{2i+1}{2} \frac{2j+1}{2} \mathcal{L}_i(u) \mathcal{L}_j(v), \quad (3b)$$

where the last sum runs over the events in the simulated sample that passes all selection criteria;

3. a combinatorial background component parameterised with a two-dimensional nonfactorisable positive polynomial function

$$\sum_{i=0}^n \sum_{j=0}^n \alpha_{ij}^2 \mathcal{B}_n^i(x) \mathcal{B}_n^j(y), \quad (4)$$

where x and y stand for the $\psi(2S)\gamma K^+$ and $\psi(2S)\gamma$ masses, reduced to the $0 \leq x, y \leq 1$ interval, $n = 2$, $\mathcal{B}_n^i(x)$ and $\mathcal{B}_n^j(y)$ are the basic Bernstein polynomials and the $(n+1)^2$ fit parameters α_{ij} are constrained such that $\sum_{ij} \alpha_{ij}^2 = 1$.

The fit model for the $B^+ \rightarrow (\chi_{c1}(3872) \rightarrow J/\psi\gamma) K^+$ decays consists of the following four components:

1. a signal component parameterised as a product of the B^+ and $\chi_{c1}(3872)$ signal shapes, where the B^+ signal shape is parameterised by the modified Gaussian function and the $\chi_{c1}(3872)$ signal shape is parameterised by a sum of the modified Gaussian function and a bifurcated Gaussian distribution [135–137];
2. a component describing the background from partially reconstructed $B \rightarrow J/\psi X$ decays, in turn consisting of two components:
 - a background from the $B^+ \rightarrow J/\psi (K^{*+} \rightarrow K^+ \pi^0)$ decay, where the shape of this component is determined from the dedicated simulated sample, following the same approach as used in Eqs. (3);
 - a background from other unidentified $B \rightarrow J/\psi X$ decays, which is parameterised by a two-dimensional Gaussian function;
3. a component describing the random $\chi_{c1}(3872)K^+$ combinations and parameterised as a product of the $\chi_{c1}(3872)$ signal shape and a constant function;

Table 2: Yields for the fit components determined from the simultaneous extended unbinned maximum-likelihood fit. Uncertainties are statistical only. The last row shows the statistical significance of the $B^+ \rightarrow (\chi_{c1}(3872) \rightarrow \psi(2S)\gamma) K^+$ signal.

| Parameter | Data-taking period | |
|--|--------------------------|------------------|
| | Run 1 | Run 2 |
| $\psi(2S)\gamma K^+$ | | |
| $N_{B^+ \rightarrow (\chi_{c1}(3872) \rightarrow \psi(2S)\gamma) K^+}$ | 40 ± 8 | 63 ± 10 |
| $N_{B \rightarrow \psi(2S) K^+ X}$ | 567 ± 24 | 885 ± 29 |
| N_{comb} | 55 ± 17 | 132 ± 19 |
| $J/\psi\gamma K^+$ | | |
| $N_{B^+ \rightarrow (\chi_{c1}(3872) \rightarrow J/\psi\gamma) K^+}$ | $[10^3]$ 0.43 ± 0.03 | 1.69 ± 0.05 |
| $N_{B \rightarrow J/\psi X}$ | $[10^3]$ 3.61 ± 0.11 | 18.72 ± 0.26 |
| $N_{\chi_{c1}(3872) K^+}$ | $[10^3]$ 1.18 ± 0.06 | 5.53 ± 0.23 |
| N_{comb} | $[10^3]$ 4.05 ± 0.11 | 17.46 ± 0.21 |
| $\mathcal{S}_{\chi_{c1}(3872) \rightarrow \psi(2S)\gamma}$ | 5.3σ | 6.7σ |

- a combinatorial background described with a nonfactorisable positive polynomial function similar to Eq. (4) with $n = 3$.

The tail and resolution parameters of the signal shapes are fixed to the values determined from simulation. The resolution parameters are further corrected by scale factors, s_{B^+} and $s_{\psi\gamma}$, which account for a small discrepancy between data and simulation [11, 51, 55, 138–141]. These factors are constrained in the fit using Gaussian constraints with values of $s_{B^+} = 1.102 \pm 0.004$ and $s_{\psi\gamma} = 1.027 \pm 0.004$, obtained from the analysis of a large sample of $B^+ \rightarrow (\chi_{c1} \rightarrow J/\psi\gamma) K^+$ decays [140].

The fit is performed simultaneously over the four samples corresponding to the $B^+ \rightarrow (\chi_{c1}(3872) \rightarrow \psi(2S)\gamma) K^+$ and $B^+ \rightarrow (\chi_{c1}(3872) \rightarrow J/\psi\gamma) K^+$ decays and the two data-taking periods. The peak position parameters of the signal shapes and the s_{B^+} and $s_{\psi\gamma}$ scale factors are shared between the samples.

The results of the fit are overlaid in Fig. 1 and the yields of each fit component are summarised in Table 2. The statistical significance for the $B^+ \rightarrow (\chi_{c1}(3872) \rightarrow \psi(2S)\gamma) K^+$ signal, $\mathcal{S}_{\chi_{c1}(3872) \rightarrow \psi(2S)\gamma}$, is calculated using Wilks' theorem [142] separately for the Run 1 and Run 2 data-taking periods and is also listed in Table 2.

To validate the observation of the $B^+ \rightarrow (\chi_{c1}(3872) \rightarrow \psi(2S)\gamma) K^+$ decay, several cross-checks are performed. The data are categorised into data-taking periods with different polarity of the LHCb dipole magnet [143] and charge of the B^\pm candidate. The results are found to be consistent among all samples. Further, alternative techniques are tried for the signal determination. Namely, instead of using fits to the two-dimensional mass distributions, fits to the one-dimensional $\psi\gamma K^+$ mass distributions are performed for events within the narrow region around the known $\chi_{c1}(3872)$ mass. The results are found to be in agreement with the baseline results. Similarly, consistent results have been obtained also from the fits to the one-dimensional $\psi\gamma$ mass distributions for events within the narrow $\psi\gamma K^+$ mass region around the known B^+ mass, when the $\psi\gamma$ mass is

calculated with $\psi\gamma K^+$ mass constrained to the known mass of the B^+ meson.

5 Branching fraction ratio computation

The ratio of the partial decay widths, $\mathcal{R}_{\psi\gamma}$, defined in Eq. (1) is calculated as

$$\mathcal{R}_{\psi\gamma} = \frac{N_{B^+ \rightarrow (\chi_{c1}(3872) \rightarrow \psi(2S)\gamma) K^+}}{N_{B^+ \rightarrow (\chi_{c1}(3872) \rightarrow J/\psi\gamma) K^+}} \times \frac{\epsilon_{B^+ \rightarrow (\chi_{c1}(3872) \rightarrow J/\psi\gamma) K^+}}{\epsilon_{B^+ \rightarrow (\chi_{c1}(3872) \rightarrow \psi(2S)\gamma) K^+}} \times \frac{\mathcal{B}_{J/\psi \rightarrow \mu^+ \mu^-}}{\mathcal{B}_{\psi(2S) \rightarrow \mu^+ \mu^-}}, \quad (5)$$

where N denotes the signal yield from Table 2, ϵ stands for the total efficiency, and \mathcal{B} is the branching fraction of a dimuon decay of the ψ mesons. The total efficiencies are the products of detector acceptance, reconstruction, selection and trigger efficiencies, and are calculated using simulated samples, calibrated to match the data as described in Sec. 2. The resulting ratios of efficiencies are found to be 3.51 ± 0.08 and 5.15 ± 0.07 for Run 1 and Run 2 data-taking periods, respectively, where the uncertainties are due to the limited size of the simulated samples. The difference between the ratios of efficiencies is mainly due to the tighter requirement on the response of the MLP classifier applied to suppress larger background for Run 2 data-taking period. Under the assumption of lepton universality, instead of the ratio of branching fractions for the dimuon decays of the J/ψ and $\psi(2S)$ mesons, the corresponding ratio for their dielectron decays of 7.53 ± 0.17 is used [120], which is known with a smaller uncertainty.

The value for the ratio $\mathcal{R}_{\psi\gamma}$ is calculated separately for the two data-taking periods and found to be

$$\begin{aligned} \mathcal{R}_{\psi\gamma}^{\text{Run 1}} &= 2.50 \pm 0.52, \\ \mathcal{R}_{\psi\gamma}^{\text{Run 2}} &= 1.49 \pm 0.23, \end{aligned}$$

where the uncertainty is statistical only. Systematic uncertainties are discussed in the next section.

6 Systematic uncertainties

The studied channels share the same set of final-state particles, trigger and preselection requirements. This leads to a significant cancellation of many systematic uncertainties in the ratio determination. The remaining contributions are discussed below and summarised in Table 3.

An important source of systematic uncertainty is associated with the fit model. The systematic uncertainty related to the description of the signal fit components is estimated using alternative models. A set of pseudoexperiments based on the baseline fit model is produced and each pseudoexperiment is fit to the alternative model and the ratio of yields for the $B^+ \rightarrow (\chi_{c1}(3872) \rightarrow \psi(2S)\gamma) K^+$ and $B^+ \rightarrow (\chi_{c1}(3872) \rightarrow J/\psi\gamma) K^+$ signal components is calculated. The mean value of this ratio from the pseudoexperiments is compared with the value from the baseline fit and the largest deviation over the considered list of alternative models is taken as the corresponding systematic uncertainty. The alternative models used for the B^+ signal shape are:

- a modified asymmetric Apollonios function [144];

Table 3: Relative systematic uncertainties (in %) in the ratio of branching fractions. The total uncertainty is obtained as the sum of individual components in quadrature.

| Source | Data-taking period | |
|---|--------------------|--------------|
| | Run 1 [%] | Run 2 [%] |
| Fit model | | |
| Signal and combinatorial background | +5.7 -0.1 | +4.4 -2.0 |
| $B \rightarrow \psi(2S)K^+X$ background | | |
| Parameterisation | +1.6 -4.9 | +5.0 -2.9 |
| Composition | 0.9 | 1.9 |
| Simulation sample size | 4.2 | 4.3 |
| Additional components | +0.6 -4.4 | +1.2 -2.6 |
| B^+ meson kinematics | < 0.1 | < 0.1 |
| Track reconstruction | < 0.1 | < 0.1 |
| Photon reconstruction | 1.1 | 1.1 |
| Kaon identification | 1.0 | 1.3 |
| Trigger | 1.1 | 1.1 |
| Data-simulation (dis)agreement | 1.0 | +1.0 -1.5 |
| Simulation sample size for efficiency | 2.3 | 1.4 |
| Total | +8.0 -9.2 | +8.7 -7.9 |

- a generalised asymmetric Student's t -distribution [145–148];
- a modified Novosibirsk function [149].

The list of alternative models for the $\chi_{c1}(3872)$ signal consists of the sum of a model from the list above with a bifurcated Gaussian distribution or the modified Gaussian function, and the sum of the modified Gaussian function with a Gaussian function. The same technique is applied to estimate the systematic uncertainty associated with parameterisation of the combinatorial background components. The two-dimensional nonfactorisable positive polynomials from Eq. (4) with $n = 1$ or $n = 3$ are tested as alternative models for the $\psi(2S)\gamma K^+$ case and with $n = 2$ for the $J/\psi\gamma K^+$ case. The largest positive and negative relative deviations over all alternative signal and combinatorial background models are found to be $^{+5.7}_{-0.1}\%$ for the Run1 and $^{+4.4}_{-2.0}\%$ for the Run2 data-taking periods, respectively. These values are taken as the corresponding systematic uncertainty.

An additional systematic uncertainty related to the description of the background from the $B \rightarrow \psi(2S)K^+X$ decays, is computed with alternative models using the technique described above. The list of alternative models consists of the two dimensional function from Eq. (3) with $n = 12$ and 15; two-dimensional histograms with different binning schemes with no interpolation, bilinear, biquadratic and bicubic interpolations. The largest positive and negative relative deviations over all alternative models are found to be $^{+1.6}_{-4.9}\%$ for the Run 1 and $^{+5.0}_{-2.9}\%$ for the Run 2 data-taking periods, respectively. These values are taken as the corresponding systematic uncertainties due to the parameterisation of the background from the $B \rightarrow \psi(2S)K^+X$ decays.

Imprecise knowledge of the branching fractions for the individual $B \rightarrow \psi(2S)K^+X$ de-

cays affects the composition of the simulated sample, and therefore the shape of the corresponding fit component. To estimate the associated systematic uncertainty, a set of dedicated pseudoexperiments is performed. For each pseudoexperiment, a set of per-event weights are derived by sampling random values from a Gaussian distribution of the known $B \rightarrow \psi(2S)K^+X$ branching fraction and its uncertainty [8, 120–122]. The weights are applied to the simulation sample and a new parameterisation of the corresponding fit component is determined for each pseudoexperiment. Subsequently, the fit is performed and the ratio of the yields for the $B^+ \rightarrow (\chi_{c1}(3872) \rightarrow \psi(2S)\gamma) K^+$ and $B^+ \rightarrow (\chi_{c1}(3872) \rightarrow J/\psi\gamma) K^+$ signals is calculated. The root mean square of the relative deviation of the ratio from the baseline fit result over the pseudoexperiments is found to be 0.9% and 1.9% for the Run 1 and Run 2 data-taking periods, which is taken as the size of the associated systematic uncertainty.

The uncertainty associated with the finite size of the simulated sample is estimated using similar types of pseudoexperiments. In each pseudoexperiment, a new dataset is drawn from the two-dimensional histogram based on the statistical uncertainty of the simulated background. The corresponding systematic uncertainty is found to be 4.2% for the Run 1 and 4.3% for Run 2 data-taking periods.

The addition of other components in the fit, namely the components describing possible contributions from random $(\chi_{c1}(3872) \rightarrow \psi(2S)\gamma) K^+$ combinations, $B^+ \rightarrow \psi(2S)\gamma K^+$ and $B^+ \rightarrow J/\psi\gamma K^+$ decays, as well as alternative parameterisation of the $(\chi_{c1}(3872) \rightarrow J/\psi\gamma) K^+$ fit component, causes only a small change with respect to the baseline result. All these components are parameterised as a product of the corresponding signal function with polynomial function up to order two. The obtained yields for all additional components are found to be small and consistent with zero, and the maximal positive and negative relative deviations with respect to the baseline fit are found to be $+0.6\%$ for Run 1 and $+1.2\%$ for Run 2 data-taking periods.

The transverse momentum and rapidity spectra for the B^+ mesons are corrected via an iterative procedure using the $B^+ \rightarrow J/\psi K^+$ control channel. The finite size of the $B^+ \rightarrow J/\psi K^+$ signal sample induces an uncertainty on the B^+ meson p_T and y spectra. In turn, this uncertainty induces a corresponding uncertainty in the ratio of efficiencies. It is estimated by using corrections from a prior iteration and checking the deviation of the ratio from the baseline value. This uncertainty is found to be smaller than 0.1% for both Run 1 and Run 2 data-taking periods.

There are residual differences in the tracking reconstruction efficiency that do not cancel out in the efficiency ratio, given the slightly different kinematic distributions of the final-state particles. The track-finding efficiencies obtained from simulated samples are corrected using $J/\psi \rightarrow \mu^+\mu^-$ calibration channels [113]. The uncertainties related to the efficiency correction factors are propagated to the ratios of the total efficiencies using pseudoexperiments, and are found to be less than 0.1% for both Run 1 and Run 2.

Differences in the photon reconstruction efficiencies between data and simulation are studied using a large sample of $B^+ \rightarrow J/\psi K^{*+}$ decays, reconstructed with the $K^{*+} \rightarrow K^+(\pi^0 \rightarrow \gamma\gamma)$ decay mode [114–118]. The uncertainty on the correction factors is propagated to the ratio of the total efficiencies using pseudoexperiments and is found to be 1.1% for both Run 1 and Run 2.

The kaon identification variable used for the MLP estimator is drawn from $D^{*+} \rightarrow (D^0 \rightarrow K^-\pi^+)\pi^+$ calibration samples [112] and has a dependence on the particle kinematics and track multiplicity in the event. Systematic uncertainties arise from

the limited size of both the simulation and calibration samples, and the modelling of the particle identification variable. The limitations due to the size of the simulation and calibration samples are evaluated by using bootstrapping techniques [150, 151] to create multiple samples and repeating the procedure for each sample. The impact of potential mismodelling of the kaon identification variable is evaluated by describing the corresponding distributions using density estimates with different kernel widths [112, 152]. For each of these cases, alternative efficiency maps are produced to determine the associated uncertainties. Systematic uncertainties of 1.0% for Run 1 and 1.3% for Run 2 are assigned from the observed differences obtained with the alternative maps.

A systematic uncertainty related to the knowledge of the trigger efficiencies was previously studied using large samples of $B^+ \rightarrow (J/\psi \rightarrow \mu^+ \mu^-) K^+$ and $B^+ \rightarrow (\psi(2S) \rightarrow \mu^+ \mu^-) K^+$ decays by comparing the ratios of the trigger efficiencies in data and simulation [153]. Based on this comparison, a relative uncertainty of 1.1% is assigned for both data-taking periods.

The remaining discrepancy between data and simulation, not explicitly covered above, is estimated using a large sample of the $B^+ \rightarrow (\chi_{c1} \rightarrow J/\psi \gamma) K^+$ decays [140]. The same preselection and MLP classifier are applied to the control channel as for the $B^+ \rightarrow (\chi_{c1}(3872) \rightarrow \psi(2S) \gamma) K^+$ channel. The systematic uncertainty is estimated by varying the requirement on the response of the MLP classifier in the full range. The resulting difference in the data-simulation efficiency ratio is found to be 1.0% in Run 1 and $^{+1.0}_{-1.5}$ % in Run 2.

The finite size of the simulation samples leads to an uncertainty on the ratios of total efficiencies, which translates to an uncertainty in the efficiency ratios of 2.3% for Run 1 and 1.4% for Run 2. The total relative systematic uncertainties on the ratio of branching fractions $\mathcal{R}_{\psi\gamma}$ are calculated as the sum in quadrature of all the values described above and are found to be $^{+8.0}_{-9.2}$ % for Run 1 and $^{+8.7}_{-7.9}$ % for Run 2.

The statistical significance of the $\chi_{c1}(3872) \rightarrow \psi(2S) \gamma$ decay is recalculated using Wilks' theorem for each alternative fit model, and the smallest values of 4.8 and 6.0 standard deviations for the Run 1 and Run 2 samples, respectively, are taken as the significance including the systematic uncertainty.

7 Results and summary

The decay $B^+ \rightarrow \chi_{c1}(3872) K^+$ is exploited to study the radiative decays of the $\chi_{c1}(3872)$ state into $\psi(2S) \gamma$ and $J/\psi \gamma$ final states using data collected by the LHCb experiment in pp collisions at centre-of-mass energies of 7, 8 and 13 TeV and corresponding to an integrated luminosity of 9 fb^{-1} . The significance of the $B^+ \rightarrow (\chi_{c1}(3872) \rightarrow \psi(2S) \gamma) K^+$ signal is found to be 4.8 and 6.0 standard deviations for the Run 1 and Run 2 data-taking periods, which is the first observation of the $\chi_{c1}(3872) \rightarrow \psi(2S) \gamma$ decay. The ratio of branching fractions for the $B^+ \rightarrow (\chi_{c1}(3872) \rightarrow \psi(2S) \gamma) K^+$ and $B^+ \rightarrow (\chi_{c1}(3872) \rightarrow J/\psi \gamma) K^+$ decays is measured separately for the Run 1 and Run 2 data-taking periods. This ratio is interpreted as the ratio of the partial decay widths for the $\chi_{c1}(3872) \rightarrow \psi \gamma$ decays from Eq. (1)

$$\begin{aligned} \mathcal{R}_{\psi\gamma}^{\text{Run 1}} &= 2.50 \pm 0.52^{+0.20}_{-0.23} \pm 0.06, \\ \mathcal{R}_{\psi\gamma}^{\text{Run 2}} &= 1.49 \pm 0.23^{+0.13}_{-0.12} \pm 0.03, \end{aligned}$$

where the first uncertainty is statistical, the second systematic and the third due to the uncertainties on the ratio of branching fractions of $\psi(2S)$ and J/ψ mesons into the dilepton final state. The ratio $\mathcal{R}_{\psi\gamma}^{\text{Run 1}}$ is in good agreement with (and supersedes) the value of $\mathcal{R}_{\psi\gamma} = 2.46 \pm 0.70$, obtained in the previous study [46]. The results for the Run 1 and Run 2 data-taking periods are combined using the best linear unbiased estimator [154] accounting for the correlated systematic uncertainties. The obtained value for the ratio $\mathcal{R}_{\psi\gamma}$ is found to be

$$\mathcal{R}_{\psi\gamma} = 1.67 \pm 0.21 \pm 0.12 \pm 0.04.$$

A summary of experimental results for the ratio of branching fractions of the $\chi_{c1}(3872) \rightarrow \psi(2S)\gamma$ and $\chi_{c1}(3872) \rightarrow J/\psi\gamma$ decays is presented in Fig. 2. The combined ratio of partial radiative widths from this study is below the upper limit set by the Belle [26] collaboration and consistent with the previous measurements by the BaBar [20] and LHCb [46] collaborations. However, it is notably in tension with the upper limit set by the BESIII collaboration [32].

The large measured value of the $\mathcal{R}_{\psi\gamma}$ ratio is generally inconsistent with the calculations based on the pure $D\bar{D}^*$ molecular hypothesis for the $\chi_{c1}(3872)$ state [59, 86, 91–93] unless some special assumptions are made [82, 83]. On the contrary, it agrees with a broad range of predictions based on other hypotheses of the $\chi_{c1}(3872)$ structure, including conventional $c\bar{c}$ charmonium [67, 69, 71, 84–90], $c\bar{c}q\bar{q}$ tetraquark [93], and molecules mixed with a sizeable compact component [82, 83, 94, 95]. This measurement provides a strong argument in favour of a compact component in the $\chi_{c1}(3872)$ structure.

Acknowledgements

We express our gratitude to our colleagues in the CERN accelerator departments for the excellent performance of the LHC. We thank the technical and administrative staff at the LHCb institutes. We acknowledge support from CERN and from the national agencies: CAPES, CNPq, FAPERJ and FINEP (Brazil); MOST and NSFC (China); CNRS/IN2P3 (France); BMBF, DFG and MPG (Germany); INFN (Italy); NWO (Netherlands); MNiSW and NCN (Poland); MCID/IFA (Romania); MICINN (Spain); SNSF and SER (Switzerland); NASU (Ukraine); STFC (United Kingdom); DOE NP and NSF (USA). We acknowledge the computing resources that are provided by CERN, IN2P3 (France), KIT and DESY (Germany), INFN (Italy), SURF (Netherlands), PIC (Spain), GridPP (United Kingdom), CSCS (Switzerland), IFIN-HH (Romania), CBPF (Brazil), and Polish WLCG (Poland). We are indebted to the communities behind the multiple open-source software packages on which we depend. Individual groups or members have received support from ARC and ARDC (Australia); Key Research Program of Frontier Sciences of CAS, CAS PIFI, CAS CCEPP, Fundamental Research Funds for the Central Universities, and Sci. & Tech. Program of Guangzhou (China); Minciencias (Colombia); EPLANET, Marie Skłodowska-Curie Actions, ERC and NextGenerationEU (European Union); A*MIDEX, ANR, IPhU and Labex P2IO, and Région Auvergne-Rhône-Alpes (France); AvH Foundation (Germany); ICSC (Italy); GVA, XuntaGal, GENCAT, Inditex, InTalent and Prog. Atracción Talento, CM (Spain); SRC (Sweden); the Leverhulme Trust, the Royal Society and UKRI (United Kingdom).

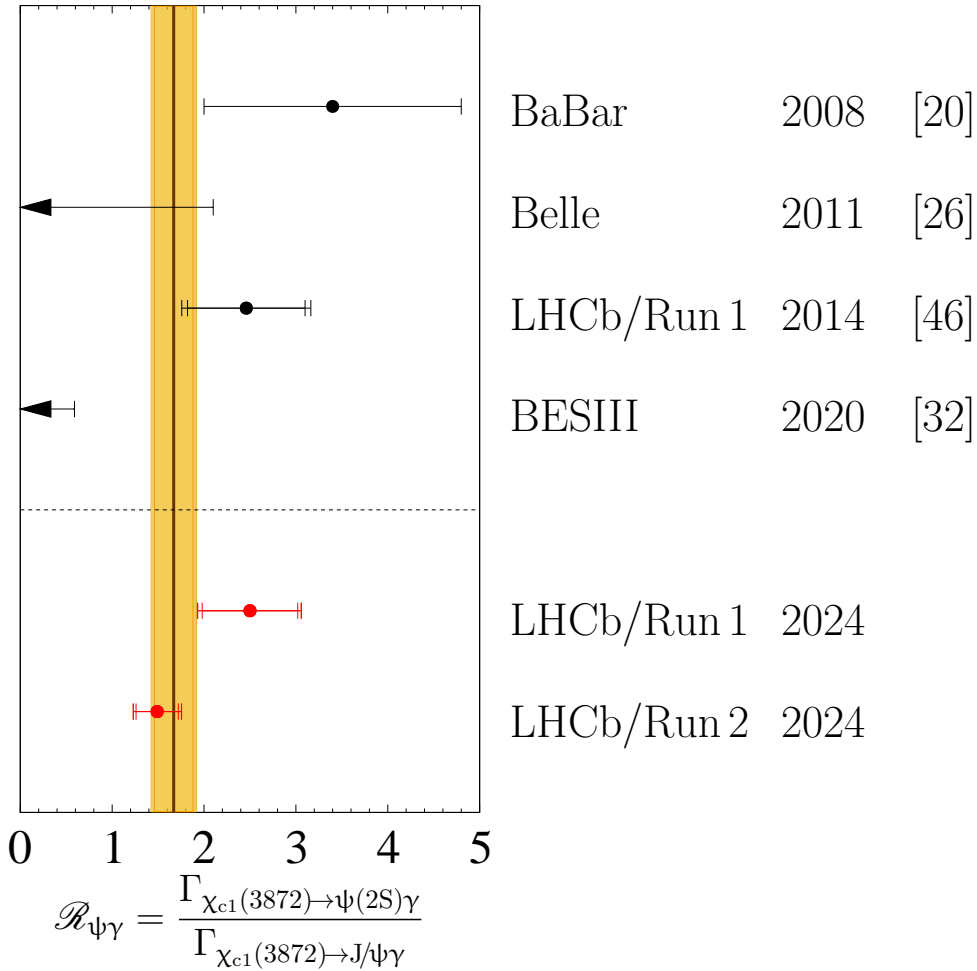


Figure 2: Summary of experimental results for the ratio of the partial decay widths for the radiative $\chi_{c1}(3872) \rightarrow \psi(2S)\gamma$ and $\chi_{c1}(3872) \rightarrow J/\psi\gamma$ decays. The results from this analysis for the Run1 and Run2 data sets are shown as red points with error bars. The coloured band corresponds to the average of the LHCb results in this paper. Where provided the outer uncertainties bars correspond to total measurement uncertainties, while inner ones are for statistical uncertainties only.

References

- [1] Belle collaboration, S. K. Choi *et al.*, *Observation of a resonance-like structure in the $\pi^\pm\psi'$ mass distribution in exclusive $B \rightarrow K\pi^\pm\psi'$ decays*, Phys. Rev. Lett. **100** (2008) 142001, [arXiv:0708.1790](#).
- [2] Belle collaboration, R. Mizuk *et al.*, *Dalitz analysis of $B \rightarrow K\pi^+\psi'$ decays and the $Z(4430)^+$* , Phys. Rev. **D80** (2009) 031104, [arXiv:0905.2869](#).
- [3] Belle collaboration, K. Chilikin *et al.*, *Experimental constraints on the spin and parity of the $Z(4430)^+$* , Phys. Rev. **D88** (2013) 074026, [arXiv:1306.4894](#).
- [4] LHCb collaboration, R. Aaij *et al.*, *Observation of the resonant character of the $Z(4430)^-$ state*, Phys. Rev. Lett. **112** (2014) 222002, [arXiv:1404.1903](#).
- [5] LHCb collaboration, R. Aaij *et al.*, *Model-independent confirmation of the $Z(4430)^-$ state*, Phys. Rev. **D92** (2015) 112009, [arXiv:1510.01951](#).
- [6] LHCb collaboration, R. Aaij *et al.*, *Evidence for exotic hadron contributions to $\Lambda_b^0 \rightarrow J/\psi p \pi^-$ decays*, Phys. Rev. Lett. **117** (2016) 082003, [arXiv:1606.06999](#).
- [7] LHCb collaboration, R. Aaij *et al.*, *Observation of exotic $J/\psi\phi$ structures from amplitude analysis of $B^+ \rightarrow J/\psi\phi K^+$ decays*, Phys. Rev. Lett. **118** (2017) 022003, [arXiv:1606.07895](#).
- [8] LHCb collaboration, R. Aaij *et al.*, *Amplitude analysis of $B^+ \rightarrow J/\psi\phi K^+$ decays*, Phys. Rev. **D95** (2017) 012002, [arXiv:1606.07898](#).
- [9] LHCb collaboration, R. Aaij *et al.*, *Evidence for an $\eta_c(1S)\pi^-$ resonance in $B^0 \rightarrow \eta_c(1S)K^+\pi^-$ decays*, Eur. Phys. J. **C78** (2018) 1019, [arXiv:1809.07416](#).
- [10] LHCb collaboration, R. Aaij *et al.*, *Model-independent observation of exotic contributions to $B^0 \rightarrow J/\psi K^+\pi^-$ decays*, Phys. Rev. Lett. **122** (2019) 152002, [arXiv:1901.05745](#).
- [11] LHCb collaboration, R. Aaij *et al.*, *Study of $B_s^0 \rightarrow J/\psi\pi^+\pi^-K^+K^-$ decays*, JHEP **02** (2021) 024, [arXiv:2011.01867](#).
- [12] LHCb collaboration, R. Aaij *et al.*, *Observation of new resonances decaying to $J/\psi K^+$ and $J/\psi\phi$* , Phys. Rev. Lett. **127** (2021) 082001, [arXiv:2103.01803](#).
- [13] Belle collaboration, S. K. Choi *et al.*, *Observation of a narrow charmonium-like state in exclusive $B^\pm \rightarrow K^\pm\pi^+\pi^-J/\psi$ decays*, Phys. Rev. Lett. **91** (2003) 262001, [arXiv:hep-ex/0309032](#).
- [14] BaBar collaboration, B. Aubert *et al.*, *Observation of the decay $B \rightarrow J/\psi\eta K$ and search for $X(3872) \rightarrow J/\psi\eta$* , Phys. Rev. Lett. **93** (2004) 041801, [arXiv:hep-ex/0402025](#).
- [15] BaBar collaboration, B. Aubert *et al.*, *Study of the $B \rightarrow J/\psi K^- \pi^+ \pi^-$ decay and measurement of the $B \rightarrow X(3872)K^-$ branching fraction*, Phys. Rev. **D71** (2005) 071103, [arXiv:hep-ex/0406022](#).

- [16] BaBar collaboration, B. Aubert *et al.*, *Search for $B^+ \rightarrow X(3872)K^+$, $X(3872) \rightarrow J/\psi\gamma$* , Phys. Rev. **D74** (2006) 071101, [arXiv:hep-ex/0607050](#).
- [17] BaBar collaboration, B. Aubert *et al.*, *Search for prompt production of χ_c and $X(3872)$ in e^+e^- annihilations*, Phys. Rev. **D76** (2007) 071102, [arXiv:0707.1633](#).
- [18] BaBar collaboration, B. Aubert *et al.*, *Study of resonances in exclusive B decays to $\bar{D}^{(*)}D^{(*)}K$* , Phys. Rev. **D77** (2008) 011102, [arXiv:0708.1565](#).
- [19] BaBar collaboration, B. Aubert *et al.*, *A Study of $B \rightarrow X(3872)K$, with $X(3872) \rightarrow J/\psi\pi^+\pi^-$* , Phys. Rev. **D77** (2008) 111101, [arXiv:0803.2838](#).
- [20] BaBar collaboration, B. Aubert *et al.*, *Evidence for $X(3872) \rightarrow \psi(2S)\gamma$ in $B^\pm \rightarrow X(3872)K^\pm$ decays, and a study of $B \rightarrow c\bar{c}\gamma K$* , Phys. Rev. Lett. **102** (2009) 132001, [arXiv:0809.0042](#).
- [21] BaBar collaboration, P. del Amo Sanchez *et al.*, *Evidence for the decay $X(3872) \rightarrow J/\psi\omega$* , Phys. Rev. **D82** (2010) 011101, [arXiv:1005.5190](#).
- [22] Belle collaboration, K. Abe *et al.*, *Observation of $B^+ \rightarrow \psi(3770)K^+$* , Phys. Rev. Lett. **93** (2004) 051803, [arXiv:hep-ex/0307061](#).
- [23] Belle collaboration, G. Gokhroo *et al.*, *Observation of a near-threshold $D^0\bar{D}^0\pi^0$ enhancement in $B \rightarrow D^0\bar{D}^0\pi^0K$ decay*, Phys. Rev. Lett. **97** (2006) 162002, [arXiv:hep-ex/0606055](#).
- [24] Belle collaboration, T. Aushev *et al.*, *Study of the $B \rightarrow X(3872) (\rightarrow D^{*0}\bar{D}^0) K$ decay*, Phys. Rev. **D81** (2010) 031103, [arXiv:0810.0358](#).
- [25] Belle collaboration, S.-K. Choi *et al.*, *Bounds on the width, mass difference and other properties of $X(3872) \rightarrow \pi^+\pi^-J/\psi$ decays*, Phys. Rev. **D84** (2011) 052004, [arXiv:1107.0163](#).
- [26] Belle collaboration, V. Bhardwaj *et al.*, *Observation of $X(3872) \rightarrow J/\psi\gamma$ and search for $X(3872) \rightarrow \psi'\gamma$ in B decays*, Phys. Rev. Lett. **107** (2011) 091803, [arXiv:1105.0177](#).
- [27] Belle collaboration, A. Bala *et al.*, *Observation of $X(3872)$ in $B \rightarrow X(3872)K\pi$ decays*, Phys. Rev. **D91** (2015) 051101, [arXiv:1501.06867](#).
- [28] Belle collaboration, J. H. Yin *et al.*, *Search for $X(3872) \rightarrow \pi^+\pi^-\pi^0$ at Belle*, Phys. Rev. **D107** (2023) 052004, [arXiv:2206.08592](#).
- [29] Belle collaboration, H. Hirata *et al.*, *Study of the lineshape of $X(3872)$ using B decays to $D^0\bar{D}^{*0}K$* , Phys. Rev. **D107** (2023) 112011, [arXiv:2302.02127](#).
- [30] BESIII collaboration, M. Ablikim *et al.*, *Observation of $e^+e^- \rightarrow \gamma X(3872)$ at BESIII*, Phys. Rev. Lett. **112** (2014) 092001, [arXiv:1310.4101](#).
- [31] BESIII collaboration, M. Ablikim *et al.*, *An improved limit for Γ_{ee} of $X(3872)$ and Γ_{ee} measurement of $\psi(3686)$* , Phys. Lett. **B749** (2015) 414, [arXiv:1505.02559](#).

- [32] BESIII collaboration, M. Ablikim *et al.*, *Study of open-charm decays and radiative transitions of the X(3872)*, Phys. Rev. Lett. **124** (2020) 242001, arXiv:2001.01156.
- [33] BESIII collaboration, M. Ablikim *et al.*, *Observation of a new X(3872) production process $e^+e^- \rightarrow \omega X(3872)$* , Phys. Rev. Lett. **130** (2023) 151904, arXiv:2212.07291.
- [34] BESIII collaboration, M. Ablikim *et al.*, *Search for the light hadron decay $\chi_{c1}(3872) \rightarrow \pi^+\pi^-\eta$* , Phys. Rev. **D109** (2024) L011102, arXiv:2308.13980.
- [35] BESIII collaboration, M. Ablikim *et al.*, *A coupled-channel analysis of the X(3872) lineshape with BESIII data*, arXiv:2309.01502.
- [36] CDF collaboration, D. Acosta *et al.*, *Observation of the narrow state $X(3872) \rightarrow J/\psi\pi^+\pi^-$ in $\bar{p}p$ collisions at $\sqrt{s} = 1.96$ TeV*, Phys. Rev. Lett. **93** (2004) 072001, arXiv:hep-ex/0312021.
- [37] CDF collaboration, A. Abulencia *et al.*, *Measurement of the dipion mass spectrum in $X(3872) \rightarrow J/\psi\pi^+\pi^-$ decays.*, Phys. Rev. Lett. **96** (2006) 102002, arXiv:hep-ex/0512074.
- [38] CDF collaboration, A. Abulencia *et al.*, *Analysis of the quantum numbers J^{PC} of the X(3872)*, Phys. Rev. Lett. **98** (2007) 132002, arXiv:hep-ex/0612053.
- [39] CDF collaboration, T. Aaltonen *et al.*, *Precision measurement of the X(3872) mass in $J/\psi\pi^+\pi^-$ decays*, Phys. Rev. Lett. **103** (2009) 152001, arXiv:0906.5218.
- [40] D0 collaboration, V. M. Abazov *et al.*, *Observation and properties of the X(3872) decaying to $J/\psi\pi^+\pi^-$ in $p\bar{p}$ collisions at $\sqrt{s} = 1.96$ TeV*, Phys. Rev. Lett. **93** (2004) 162002, arXiv:hep-ex/0405004.
- [41] ATLAS collaboration, M. Aaboud *et al.*, *Measurements of $\psi(2S)$ and $X(3872) \rightarrow J/\psi\pi^+\pi^-$ production in pp collisions at $\sqrt{s} = 8$ TeV with the ATLAS detector*, JHEP **01** (2017) 117, arXiv:1610.09303.
- [42] CMS collaboration, S. Chatrchyan *et al.*, *Measurement of the X(3872) production cross section via decays to $J/\psi\pi^+\pi^-$ in pp collisions at $\sqrt{s} = 7$ TeV*, JHEP **04** (2013) 154, arXiv:1302.3968.
- [43] CMS collaboration, A. M. Sirunyan *et al.*, *Observation of the $B_s^0 \rightarrow X(3872)\phi$ decay*, Phys. Rev. Lett. **125** (2020) 152001, arXiv:2005.04764.
- [44] LHCb collaboration, R. Aaij *et al.*, *Observation of X(3872) production in pp collisions at $\sqrt{s} = 7$ TeV*, Eur. Phys. J. **C72** (2012) 1972, arXiv:1112.5310.
- [45] LHCb collaboration, R. Aaij *et al.*, *Determination of the X(3872) meson quantum numbers*, Phys. Rev. Lett. **110** (2013) 222001, arXiv:1302.6269.
- [46] LHCb collaboration, R. Aaij *et al.*, *Evidence for the decay $X(3872) \rightarrow \psi(2S)\gamma$* , Nucl. Phys. **B886** (2014) 665, arXiv:1404.0275.
- [47] LHCb collaboration, R. Aaij *et al.*, *Quantum numbers of the X(3872) state and orbital angular momentum in its $\rho^0 J/\psi$ decays*, Phys. Rev. **D92** (2015) 011102(R), arXiv:1504.06339.

- [48] LHCb collaboration, R. Aaij *et al.*, *Observation of $\eta_c(2S) \rightarrow p\bar{p}$ and search for $X(3872) \rightarrow p\bar{p}$ decays*, Phys. Lett. **B769** (2017) 305, [arXiv:1607.06446](#).
- [49] LHCb collaboration, R. Aaij *et al.*, *Observation of the $\Lambda_b^0 \rightarrow \chi_{c1}(3872)pK^-$ decay*, JHEP **09** (2019) 028, [arXiv:1907.00954](#).
- [50] LHCb collaboration, R. Aaij *et al.*, *Study of the line shape of the $\chi_{c1}(3872)$ state*, Phys. Rev. **D102** (2020) 092005, [arXiv:2005.13419](#).
- [51] LHCb collaboration, R. Aaij *et al.*, *Study of the $\psi_2(3823)$ and $\chi_{c1}(3872)$ states in $B^+ \rightarrow (J/\psi\pi^+\pi^-)K^+$ decays*, JHEP **08** (2020) 123, [arXiv:2005.13422](#).
- [52] LHCb collaboration, R. Aaij *et al.*, *Observation of multiplicity-dependent $\chi_{c1}(3872)$ and $\psi(2S)$ production in pp collisions*, Phys. Rev. Lett. **126** (2021) 092001, [arXiv:2009.06619](#).
- [53] LHCb collaboration, R. Aaij *et al.*, *Measurement of $\chi_{c1}(3872)$ production in proton-proton collisions at $\sqrt{s} = 8$ and 13 TeV*, JHEP **01** (2022) 131, [arXiv:2109.07360](#).
- [54] LHCb collaboration, R. Aaij *et al.*, *Observation of sizeable ω contribution to $\chi_{c1}(3872) \rightarrow \pi^+\pi^-J/\psi$ decays*, Phys. Rev. **D108** (2023) L011103, [arXiv:2204.12597](#).
- [55] LHCb collaboration, R. Aaij *et al.*, *Study of charmonium and charmonium-like contributions in $B^+ \rightarrow J/\psi\eta K^+$ decays*, JHEP **04** (2021) 46, [arXiv:2202.04045](#).
- [56] LHCb collaboration, R. Aaij *et al.*, *Modification of $\chi_{c1}(3872)$ and $\psi(2S)$ production in pPb collisions at $\sqrt{s_{NN}} = 8.16$ TeV*, [arXiv:2402.14975](#), submitted to Phys. Rev. Lett.
- [57] CMS collaboration, A. M. Sirunyan *et al.*, *Evidence for $X(3872)$ in Pb–Pb collisions and studies of its prompt production at $\sqrt{s_{NN}} = 5.02$ TeV*, Phys. Rev. Lett. **128** (2022) 032001, [arXiv:2102.13048](#).
- [58] E. Braaten and M. Kusunoki, *Low-energy universality and the new charmonium resonance at 3870 MeV*, Phys. Rev. **D69** (2004) 074005, [arXiv:hep-ph/0311147](#).
- [59] E. S. Swanson, *Short range structure in the $X(3872)$* , Phys. Lett. **B588** (2004) 189, [arXiv:hep-ph/0311229](#).
- [60] C.-Y. Wong, *Molecular states of heavy quark mesons*, Phys. Rev. **C69** (2004) 055202, [arXiv:hep-ph/0311088](#).
- [61] N. A. Tornqvist, *Isospin breaking of the narrow charmonium state of Belle at 3872 MeV as a deuson*, Phys. Lett. **B590** (2004) 209, [arXiv:hep-ph/0402237](#).
- [62] C. Hanhart, Y. S. Kalashnikova, A. E. Kudryavtsev, and A. V. Nefediev, *Reconciling the $X(3872)$ with the near-threshold enhancement in the $D^0\bar{D}^{*0}$ final state*, Phys. Rev. **D76** (2007) 034007, [arXiv:0704.0605](#).

- [63] P. Artoisenet and E. Braaten, *Production of the X(3872) at the Tevatron and the LHC*, Phys. Rev. **D81** (2010) 114018, arXiv:0911.2016.
- [64] C. Bignamini *et al.*, *Is the X(3872) production cross section at Tevatron compatible with a hadron molecule interpretation?*, Phys. Rev. Lett. **103** (2009) 162001, arXiv:0906.0882.
- [65] A. Esposito *et al.*, *Observation of light nuclei at ALICE and the X(3872) conundrum*, Phys. Rev. **D92** (2015) 034028, arXiv:1508.00295.
- [66] Z.-L. She *et al.*, *Identifying X(3872) molecular state or the tetraquark state in pp collisions with PACIAE 3.0*, arXiv:2402.16736.
- [67] T. Barnes and S. Godfrey, *Charmonium options for the X(3872)*, Phys. Rev. **D69** (2004) 054008, arXiv:hep-ph/0311162.
- [68] E. J. Eichten, K. Lane, and C. Quigg, *Charmonium levels near threshold and the narrow state X(3872) $\rightarrow \pi^+\pi^-J/\psi$* , Phys. Rev. **D69** (2004) 094019, arXiv:hep-ph/0401210.
- [69] T. Barnes, S. Godfrey, and E. S. Swanson, *Higher charmonia*, Phys. Rev. **D72** (2005) 054026, arXiv:hep-ph/0505002.
- [70] M. Suzuki, *The X(3872) boson: molecule or charmonium*, Phys. Rev. **D72** (2005) 114013, arXiv:hep-ph/0508258.
- [71] F. Giacosa, M. Piotrowska, and S. Coito, *X(3872) as virtual companion pole of the charm-anticharm state $\chi_{c1}(2P)$* , Int. J. Mod. Phys. **A34** (2019) 1950173, arXiv:1903.06926.
- [72] F. E. Close and P. R. Page, *The $D^0\bar{D}^{*0}$ threshold resonance*, Phys. Lett. **B578** (2004) 119, arXiv:hep-ph/0309253.
- [73] S. Dubynskiy and M. B. Voloshin, *Hadro-charmonium*, Phys. Lett. **B666** (2008) 344, arXiv:0803.2224.
- [74] F. E. Close and S. Godfrey, *Charmonium hybrid production in exclusive B meson decays*, Phys. Lett. **B574** (2003) 210, arXiv:hep-ph/0305285.
- [75] B. A. Li, *Is X(3872) a possible candidate of hybrid meson*, Phys. Lett. **B605** (2005) 306, arXiv:hep-ph/0410264.
- [76] L. Maiani, F. Piccinini, A. D. Polosa, and V. Riquer, *Diquark-antidiquarks with hidden or open charm and the nature of X(3872)*, Phys. Rev. **D71** (2005) 014028, arXiv:hep-ph/0412098.
- [77] R. D. Matheus, S. Narison, M. Nielsen, and J. M. Richard, *Can the X(3872) be a 1^{++} four-quark state?*, Phys. Rev. **D75** (2007) 014005, arXiv:hep-ph/0608297.
- [78] S. Weinberg, *Evidence that the deuteron is not an elementary particle*, Phys. Rev. **137** (1965) B672.


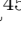






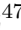




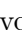
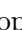





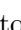




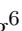
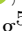
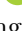



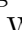













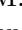




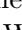

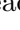

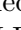


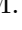
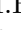
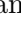






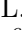
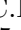

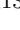

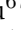
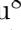
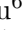
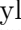
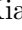
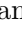






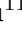
















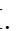









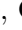





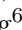
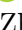






- [79] A. Esposito *et al.*, *From the line shape of the X(3872) to its structure*, Phys. Rev. **D105** (2022) L031503, [arXiv:2108.11413](#).
- [80] A. Esposito *et al.*, *The role of the pion in the lineshape of the X(3872)*, Phys. Lett. **847** (2023) 138285, [arXiv:2307.11400](#).
- [81] E. S. Swanson, *Diagnostic decays of the X(3872)*, Phys. Lett. **B598** (2004) 197, [arXiv:hep-ph/0406080](#).
- [82] F.-K. Guo *et al.*, *What can radiative decays of the X(3872) teach us about its nature?*, Phys. Lett. **B742** (2015) 394, [arXiv:1410.6712](#).
- [83] D. A. S. Molnar, R. F. Luiz, and R. Higa, *Short-distance RG-analysis of X(3872) radiative decays*, [arXiv:1601.03366](#).
- [84] F. De Fazio, *Radiative transitions of heavy quarkonium states*, Phys. Rev. **D79** (2009) 054015, Erratum *ibid.* **D83** (2011) 099901, [arXiv:0812.0716](#).
- [85] B.-Q. Li and K.-T. Chao, *Higher Charmonia and X, Y, Z states with screened potential*, Phys. Rev. **D79** (2009) 094004, [arXiv:0903.5506](#).
- [86] Y. Dong, A. Faessler, T. Gutsche, and V. E. Lyubovitskij, *J/ψγ and ψ(2S)γ decay modes of the X(3872)*, J. Phys. **G38** (2011) 015001, [arXiv:0909.0380](#).
- [87] A. M. Badalian, V. D. Orlovsky, Y. A. Simonov, and B. L. G. Bakker, *The ratio of decay widths of X(3872) to ψ'γ and J/ψγ as a test of the X(3872) dynamical structure*, Phys. Rev. **D85** (2012) 114002, [arXiv:1202.4882](#).
- [88] J. Ferretti, G. Galatà, and E. Santopinto, *Quark structure of the X(3872) and χ_b(3P) resonances*, Phys. Rev. **D90** (2014) 054010, [arXiv:1401.4431](#).
- [89] A. M. Badalian, Y. A. Simonov, and B. L. G. Bakker, *c \bar{c} interaction above threshold and the radiative decay X(3872) → J/ψγ*, Phys. Rev. **D91** (2015) 056001, [arXiv:1501.01168](#).
- [90] W.-J. Deng, H. Liu, L.-C. Gui, and X.-H. Zhong, *Charmonium spectrum and their electromagnetic transitions with higher multipole contributions*, Phys. Rev. **D95** (2017) 034026, [arXiv:1608.00287](#).
- [91] D. P. Rathaud and A. K. Rai, *Dimesonic states with the heavy-light flavour mesons*, Eur. Phys. J. Plus **132** (2017) 370, [arXiv:1608.03781](#).
- [92] R. F. Lebed and S. R. Martinez, *Adiabatic representation of exotic hadrons in the dynamical diquark model*, Phys. Rev. **D106** (2022) 074007, [arXiv:2207.01101](#).
- [93] B. Grinstein, L. Maiani, and A. D. Polosa, *Radiative decays of X(3872) discriminate between the molecular and compact interpretations*, Phys. Rev. **D109** (2024) 074009, [arXiv:2401.11623](#).
- [94] E. Cincioglu, J. Nieves, A. Ozpineci, and A. U. Yilmazer, *Quarkonium contribution to meson molecules*, Eur. Phys. J. **C76** (2016) 576, [arXiv:1606.03239](#).

- [95] S. Takeuchi, M. Takizawa, and K. Shimizu, *Radiative decays of the X(3872) in the charmonium-molecule hybrid picture*, JPS Conf. Proc. **17** (2017) 112001, [arXiv:1602.04297](#).
- [96] LHCb collaboration, A. A. Alves Jr. *et al.*, *The LHCb detector at the LHC*, JINST **3** (2008) S08005.
- [97] LHCb collaboration, R. Aaij *et al.*, *LHCb detector performance*, Int. J. Mod. Phys. **A30** (2015) 1530022, [arXiv:1412.6352](#).
- [98] R. Aaij *et al.*, *Performance of the LHCb Vertex Locator*, JINST **9** (2014) P09007, [arXiv:1405.7808](#).
- [99] R. Arink *et al.*, *Performance of the LHCb Outer Tracker*, JINST **9** (2014) P01002, [arXiv:1311.3893](#).
- [100] P. d'Argent *et al.*, *Improved performance of the LHCb Outer Tracker in LHC Run 2*, JINST **12** (2017) P11016, [arXiv:1708.00819](#).
- [101] M. Adinolfi *et al.*, *Performance of the LHCb RICH detector at the LHC*, Eur. Phys. J. **C73** (2013) 2431, [arXiv:1211.6759](#).
- [102] A. A. Alves Jr. *et al.*, *Performance of the LHCb muon system*, JINST **8** (2013) P02022, [arXiv:1211.1346](#).
- [103] R. Aaij *et al.*, *The LHCb trigger and its performance in 2011*, JINST **8** (2013) P04022, [arXiv:1211.3055](#).
- [104] R. Aaij *et al.*, *Performance of the LHCb trigger and full real-time reconstruction in Run 2 of the LHC*, JINST **14** (2019) P04013, [arXiv:1812.10790](#).
- [105] T. Sjöstrand, S. Mrenna, and P. Skands, *A brief introduction to PYTHIA 8.1*, Comput. Phys. Commun. **178** (2008) 852, [arXiv:0710.3820](#).
- [106] I. Belyaev *et al.*, *Handling of the generation of primary events in GAUSS, the LHCb simulation framework*, J. Phys. Conf. Ser. **331** (2011) 032047.
- [107] D. J. Lange, *The EvtGen particle decay simulation package*, Nucl. Instrum. Meth. **A462** (2001) 152.
- [108] N. Davidson, T. Przedzinski, and Z. Was, *PHOTOS interface in C++: Technical and physics documentation*, Comp. Phys. Comm. **199** (2016) 86, [arXiv:1011.0937](#).
- [109] Geant4 collaboration, S. Agostinelli *et al.*, *GEANT4: A simulation toolkit*, Nucl. Instrum. Meth. **A506** (2003) 250.
- [110] Geant4 collaboration, J. Allison *et al.*, *GEANT4 developments and applications*, IEEE Trans. Nucl. Sci. **53** (2006) 270.
- [111] M. Clemencic *et al.*, *The LHCb simulation application, GAUSS: Design, evolution and experience*, J. Phys. Conf. Ser. **331** (2011) 032023.

- [112] R. Aaij *et al.*, *Selection and processing of calibration samples to measure the particle identification performance of the LHCb experiment in Run 2*, Eur. Phys. J. Tech. Instr. **6** (2019) 1, arXiv:1803.00824.
- [113] LHCb collaboration, R. Aaij *et al.*, *Measurement of the track reconstruction efficiency at LHCb*, JINST **10** (2015) P02007, arXiv:1408.1251.
- [114] LHCb collaboration, R. Aaij *et al.*, *Evidence for the decay $B^0 \rightarrow J/\psi\omega$ and measurement of the relative branching fractions of B_s^0 meson decays to $J/\psi\eta$ and $J/\psi\eta'$* , Nucl. Phys. **B867** (2013) 547, arXiv:1210.2631.
- [115] LHCb collaboration, R. Aaij *et al.*, *Observations of $B_s^0 \rightarrow \psi(2S)\eta$ and $B_{(s)}^0 \rightarrow \psi(2S)\pi^+\pi^-$ decays*, Nucl. Phys. **B871** (2013) 403, arXiv:1302.6354.
- [116] E. Govorkova, *Study of π^0/γ efficiency using B meson decays in the LHCb experiment*, Phys. Atom. Nucl. **79** (2016) 1474, arXiv:1505.02960.
- [117] K. Govorkova, *Study of photons and neutral pions reconstruction efficiency in the LHCb experiment*, 2015. CERN-THESIS-2015-272.
- [118] I. M. Belyaev, E. M. Govorkova, V. Y. Egorychev, and D. V. Savrina, *Study of π^0/γ reconstruction and selection efficiency in the LHCb experiment*, Moscow Univ. Phys. Bull. **70** (2015) 497.
- [119] LHCb collaboration, R. Aaij *et al.*, *Measurement of the polarization amplitudes in $B^0 \rightarrow J/\psi K^*(892)^0$ decays*, Phys. Rev. **D88** (2013) 052002, arXiv:1307.2782.
- [120] Particle Data Group, R. L. Workman *et al.*, *Review of particle physics*, Prog. Theor. Exp. Phys. **2022** (2022) 083C01.
- [121] Belle collaboration, H. Guler *et al.*, *Study of the $K^+\pi^+\pi^-$ final state in $B^+ \rightarrow J/\psi K^+\pi^+\pi^-$ and $B^+ \rightarrow \psi(2S)K^+\pi^+\pi^-$* , Phys. Rev. **D83** (2011) 032005, arXiv:1009.5256.
- [122] Belle collaboration, K. Chilikin *et al.*, *Experimental constraints on the spin and parity of the $Z(4430)^+$* , Phys. Rev. **D88** (2013) 074026, arXiv:1306.4894.
- [123] LHCb collaboration, R. Aaij *et al.*, *Observation of the decay $\Lambda_b^0 \rightarrow \chi_{c1}p\pi^-$* , JHEP **05** (2021) 095, arXiv:2103.04949.
- [124] A. Powell *et al.*, *Particle identification at LHCb*, PoS **ICHEP2010** (2010) 020, LHCb-PROC-2011-008.
- [125] O. Deschamps *et al.*, *Photon and neutral pion reconstruction*, LHCb-2003-091, 2003.
- [126] H. Terrier and I. Belyaev, *Particle identification with LHCb calorimeters*, LHCb-2003-092, 2003.
- [127] C. Abellan Beteta *et al.*, *Calibration and performance of the LHCb calorimeters in Run 1 and 2 at the LHC*, arXiv:2008.11556, submitted to JINST.

- [128] W. D. Hulsbergen, *Decay chain fitting with a Kalman filter*, Nucl. Instrum. Meth. **A552** (2005) 566, [arXiv:physics/0503191](#).
- [129] W. S. McCulloch and W. Pitts, *A logical calculus of the ideas immanent in nervous activity*, The bulletin of mathematical biophysics **5** (1943) 115.
- [130] F. Rosenblatt, *The perceptron: A probabilistic model for information storage and organization in the brain*, Psychological Review **65** (1958) 386.
- [131] J.-H. Zhong *et al.*, *A program for the Bayesian neural network in the ROOT framework*, Comput. Phys. Commun. **182** (2011) 2655, [arXiv:1103.2854](#).
- [132] S. Geisser, *Predictive inference: An introduction*, Chapman and Hall/CRC, New York, 1993.
- [133] T. Skwarnicki, *A study of the radiative cascade transitions between the Υ' and Υ resonances*, PhD thesis, Institute of Nuclear Physics, Krakow, 1986, DESY-F31-86-02.
- [134] LHCb collaboration, R. Aaij *et al.*, *Observation of J/ψ -pair production in pp collisions at $\sqrt{s} = 7$ TeV*, Phys. Lett. **B707** (2012) 52, [arXiv:1109.0963](#).
- [135] G. T. Fechner, *Kollektivmasslehre*, Wilhelm Engelmann, Leipzig, 1897. Published posthumously, completed and edited by G. F. Lipps.
- [136] J. F. Gibbons and S. Mylroie, *Estimation of impurity profiles in ion-implanted amorphous targets using joined half-Gaussian distributions*, Applied Phys. Lett. **22** (1973) 568–569.
- [137] S. John, *The three-parameter two-piece normal family of distributions and its fitting*, Communications in Statistics **11** (1982) 879.
- [138] LHCb collaboration, R. Aaij *et al.*, *Study of B_c^+ decays to charmonia and three light hadrons*, JHEP **01** (2022) 065, [arXiv:2111.03001](#).
- [139] LHCb collaboration, R. Aaij *et al.*, *Study of B_c^+ decays to charmonia plus multihadron final states*, JHEP **07** (2023) 198, [arXiv:2208.08660](#).
- [140] LHCb collaboration, R. Aaij *et al.*, *Study of $B_c^+ \rightarrow \chi_c \pi^+$ decays*, JHEP **2024** (2024) 173, [arXiv:2312.12987](#).
- [141] LHCb collaboration, R. Aaij *et al.*, *Observation of the $B_c^+ \rightarrow J/\psi \pi^+ \pi^0$ decay*, JHEP **04** (2024) 151, [arXiv:2402.05523](#).
- [142] S. S. Wilks, *The large-sample distribution of the likelihood ratio for testing composite hypotheses*, Ann. Math. Stat. **9** (1938) 60.
- [143] LHCb collaboration, *LHCb magnet: Technical Design Report*, CERN-LHCC-2000-007, 2000.
- [144] D. Martínez Santos and F. Dupertuis, *Mass distributions marginalized over per-event errors*, Nucl. Instrum. Meth. **A764** (2014) 150, [arXiv:1312.5000](#).
- [145] Student (W. S. Gosset), *The probable error of a mean*, Biometrika **6** (1908) 1.

- [146] S. Jackman, *Bayesian analysis for the social sciences*, John Wiley & Sons, Inc., Hoboken, New Jersey, USA, 2009.
- [147] D. Zhu and J. W. Galbraith, *A generalized asymmetric Student-t distribution with application to financial econometrics*, *Journal of Econometrics* **157** (2010) 297.
- [148] R. Li and S. Nadarajah, *A review of Student's t-distribution and its generalizations*, *Empir. Econ.* **48** (2020) 1461.
- [149] BaBar collaboration, J. P. Lees *et al.*, *Branching fraction measurements of the color-suppressed decays $\bar{B}^0 \rightarrow D^{(*)0}\pi^0$, $D^{(*)0}\eta$, $D^{(*)0}\omega$, and $D^{(*)0}\eta'$ and measurement of the polarization in the decay $\bar{B}^0 \rightarrow D^{*0}\omega$* , *Phys. Rev.* **D84** (2011) 112007, Erratum *ibid.* **D87** (2013) 039901, [arXiv:1107.5751](#).
- [150] B. Efron, *Bootstrap methods: Another look at the jackknife*, *Ann. Statist.* **7** (1979) 1.
- [151] B. Efron and R. J. Tibshirani, *An introduction to the bootstrap*, Chapman and Hall, New York, 1994.
- [152] A. Poluektov, *Kernel density estimation of a multidimensional efficiency profile*, *JINST* **10** (2015) P02011, [arXiv:1411.5528](#).
- [153] LHCb collaboration, R. Aaij *et al.*, *Measurement of relative branching fractions of B decays to $\psi(2S)$ and J/ψ mesons*, *Eur. Phys. J.* **C72** (2012) 2118, [arXiv:1205.0918](#).
- [154] L. Lyons, D. Gibaut, and P. Clifford, *How to combine correlated estimates of a single physical quantity*, *Nucl. Instrum. Meth.* **A270** (1988) 110.

P. Vazquez Regueiro⁴⁵ , C. Vázquez Sierra⁴⁵ , S. Vecchi²⁴ , J.J. Velthuis⁵³ ,
M. Veltri^{25,w} , A. Venkateswaran⁴⁸ , M. Vesterinen⁵⁵ , D. Vico Benet⁶² ,
M. Vieites Diaz⁴⁷ , X. Vilasis-Cardona⁴³ , E. Vilella Figueras⁵⁹ , A. Villa²³ ,
P. Vincent¹⁵ , F.C. Volle⁵² , D. vom Bruch¹² , N. Voropaev⁴² , K. Vos⁷⁷ ,
G. Vouters^{10,47} , C. Vrahas⁵⁷ , J. Wagner¹⁸ , J. Walsh³³ , E.J. Walton^{1,55} , G. Wan⁶ ,
C. Wang²⁰ , G. Wang⁸ , J. Wang⁶ , J. Wang⁵ , J. Wang⁴ , J. Wang⁷² , M. Wang²⁸ ,
N. W. Wang⁷ , R. Wang⁵³ , X. Wang⁸ , X. Wang⁷⁰ , X. W. Wang⁶⁰ , Y. Wang⁶ ,
Z. Wang¹³ , Z. Wang⁴ , Z. Wang²⁸ , J.A. Ward^{55,1} , M. Waterlaet⁴⁷ , N.K. Watson⁵² ,
D. Websdale⁶⁰ , Y. Wei⁶ , J. Wendel⁷⁹ , B.D.C. Westhenry⁵³ , C. White⁵⁴ ,
M. Whitehead⁵⁸ , E. Whiter⁵² , A.R. Wiederhold⁵⁵ , D. Wiedner¹⁸ , G. Wilkinson⁶² ,
M.K. Wilkinson⁶⁴ , M. Williams⁶³ , M.R.J. Williams⁵⁷ , R. Williams⁵⁴ , Z.
Williams⁵³ , F.F. Wilson⁵⁶ , W. Wislicki⁴⁰ , M. Witek³⁹ , L. Witola²⁰ , C.P. Wong⁶⁶ ,
G. Wormser¹³ , S.A. Wotton⁵⁴ , H. Wu⁶⁷ , J. Wu⁸ , Y. Wu⁶ , K. Wyllie⁴⁷ , S. Xian⁷⁰ ,
Z. Xiang⁵ , Y. Xie⁸ , A. Xu³³ , J. Xu⁷ , L. Xu⁴ , L. Xu⁴ , M. Xu⁵⁵ , Z. Xu¹¹ ,
Z. Xu⁷ , Z. Xu⁵ , D. Yang , K. Yang⁶⁰ , S. Yang⁷ , X. Yang⁶ , Y. Yang^{27,m} ,
Z. Yang⁶ , Z. Yang⁶⁵ , V. Yeroshenko¹³ , H. Yeung⁶¹ , H. Yin⁸ , C. Y. Yu⁶ ,
J. Yu⁶⁹ , X. Yuan⁵ , Y. Yuan^{5,7} , E. Zaffaroni⁴⁸ , M. Zavertyaev¹⁹ , M. Zdybal³⁹ , C.
Zeng^{5,7} , M. Zeng⁴ , C. Zhang⁶ , D. Zhang⁸ , J. Zhang⁷ , L. Zhang⁴ , S. Zhang⁶⁹ ,
S. Zhang⁶² , Y. Zhang⁶ , Y. Z. Zhang⁴ , Y. Zhao²⁰ , A. Zharkova⁴² , A. Zhelezov²⁰ ,
S. Z. Zheng⁶ , X. Z. Zheng⁴ , Y. Zheng⁷ , T. Zhou⁶ , X. Zhou⁸ , Y. Zhou⁷ ,
V. Zhovkovska⁵⁵ , L. Z. Zhu⁷ , X. Zhu⁴ , X. Zhu⁸ , V. Zhukov¹⁶ , J. Zhuo⁴⁶ ,
Q. Zou^{5,7} , D. Zuliani^{31,p} , G. Zunica⁴⁸ .

¹*School of Physics and Astronomy, Monash University, Melbourne, Australia*

²*Centro Brasileiro de Pesquisas Físicas (CBPF), Rio de Janeiro, Brazil*

³*Universidade Federal do Rio de Janeiro (UFRJ), Rio de Janeiro, Brazil*

⁴*Center for High Energy Physics, Tsinghua University, Beijing, China*

⁵*Institute Of High Energy Physics (IHEP), Beijing, China*

⁶*School of Physics State Key Laboratory of Nuclear Physics and Technology, Peking University, Beijing, China*

⁷*University of Chinese Academy of Sciences, Beijing, China*

⁸*Institute of Particle Physics, Central China Normal University, Wuhan, Hubei, China*

⁹*Consejo Nacional de Rectores (CONARE), San Jose, Costa Rica*

¹⁰*Université Savoie Mont Blanc, CNRS, IN2P3-LAPP, Annecy, France*

¹¹*Université Clermont Auvergne, CNRS/IN2P3, LPC, Clermont-Ferrand, France*

¹²*Aix Marseille Univ, CNRS/IN2P3, CPPM, Marseille, France*

¹³*Université Paris-Saclay, CNRS/IN2P3, IJCLab, Orsay, France*

¹⁴*Laboratoire Leprince-Ringuet, CNRS/IN2P3, Ecole Polytechnique, Institut Polytechnique de Paris, Palaiseau, France*

¹⁵*LPNHE, Sorbonne Université, Paris Diderot Sorbonne Paris Cité, CNRS/IN2P3, Paris, France*

¹⁶*I. Physikalisches Institut, RWTH Aachen University, Aachen, Germany*

¹⁷*Universität Bonn - Helmholtz-Institut für Strahlen und Kernphysik, Bonn, Germany*

¹⁸*Fakultät Physik, Technische Universität Dortmund, Dortmund, Germany*

¹⁹*Max-Planck-Institut für Kernphysik (MPIK), Heidelberg, Germany*

²⁰*Physikalisches Institut, Ruprecht-Karls-Universität Heidelberg, Heidelberg, Germany*

²¹*School of Physics, University College Dublin, Dublin, Ireland*

²²*INFN Sezione di Bari, Bari, Italy*

²³*INFN Sezione di Bologna, Bologna, Italy*

²⁴*INFN Sezione di Ferrara, Ferrara, Italy*

²⁵*INFN Sezione di Firenze, Firenze, Italy*

²⁶*INFN Laboratori Nazionali di Frascati, Frascati, Italy*

²⁷*INFN Sezione di Genova, Genova, Italy*

²⁸*INFN Sezione di Milano, Milano, Italy*

²⁹*INFN Sezione di Milano-Bicocca, Milano, Italy*

- ³⁰ INFN Sezione di Cagliari, Monserrato, Italy
- ³¹ INFN Sezione di Padova, Padova, Italy
- ³² INFN Sezione di Perugia, Perugia, Italy
- ³³ INFN Sezione di Pisa, Pisa, Italy
- ³⁴ INFN Sezione di Roma La Sapienza, Roma, Italy
- ³⁵ INFN Sezione di Roma Tor Vergata, Roma, Italy
- ³⁶ Nikhef National Institute for Subatomic Physics, Amsterdam, Netherlands
- ³⁷ Nikhef National Institute for Subatomic Physics and VU University Amsterdam, Amsterdam, Netherlands
- ³⁸ AGH - University of Krakow, Faculty of Physics and Applied Computer Science, Kraków, Poland
- ³⁹ Henryk Niewodniczanski Institute of Nuclear Physics Polish Academy of Sciences, Kraków, Poland
- ⁴⁰ National Center for Nuclear Research (NCBJ), Warsaw, Poland
- ⁴¹ Horia Hulubei National Institute of Physics and Nuclear Engineering, Bucharest-Magurele, Romania
- ⁴² Affiliated with an institute covered by a cooperation agreement with CERN
- ⁴³ DS4DS, La Salle, Universitat Ramon Llull, Barcelona, Spain
- ⁴⁴ ICCUB, Universitat de Barcelona, Barcelona, Spain
- ⁴⁵ Instituto Galego de Física de Altas Enerxías (IGFAE), Universidade de Santiago de Compostela, Santiago de Compostela, Spain
- ⁴⁶ Instituto de Física Corpuscular, Centro Mixto Universidad de Valencia - CSIC, Valencia, Spain
- ⁴⁷ European Organization for Nuclear Research (CERN), Geneva, Switzerland
- ⁴⁸ Institute of Physics, Ecole Polytechnique Fédérale de Lausanne (EPFL), Lausanne, Switzerland
- ⁴⁹ Physik-Institut, Universität Zürich, Zürich, Switzerland
- ⁵⁰ NSC Kharkiv Institute of Physics and Technology (NSC KIPT), Kharkiv, Ukraine
- ⁵¹ Institute for Nuclear Research of the National Academy of Sciences (KINR), Kyiv, Ukraine
- ⁵² University of Birmingham, Birmingham, United Kingdom
- ⁵³ H.H. Wills Physics Laboratory, University of Bristol, Bristol, United Kingdom
- ⁵⁴ Cavendish Laboratory, University of Cambridge, Cambridge, United Kingdom
- ⁵⁵ Department of Physics, University of Warwick, Coventry, United Kingdom
- ⁵⁶ STFC Rutherford Appleton Laboratory, Didcot, United Kingdom
- ⁵⁷ School of Physics and Astronomy, University of Edinburgh, Edinburgh, United Kingdom
- ⁵⁸ School of Physics and Astronomy, University of Glasgow, Glasgow, United Kingdom
- ⁵⁹ Oliver Lodge Laboratory, University of Liverpool, Liverpool, United Kingdom
- ⁶⁰ Imperial College London, London, United Kingdom
- ⁶¹ Department of Physics and Astronomy, University of Manchester, Manchester, United Kingdom
- ⁶² Department of Physics, University of Oxford, Oxford, United Kingdom
- ⁶³ Massachusetts Institute of Technology, Cambridge, MA, United States
- ⁶⁴ University of Cincinnati, Cincinnati, OH, United States
- ⁶⁵ University of Maryland, College Park, MD, United States
- ⁶⁶ Los Alamos National Laboratory (LANL), Los Alamos, NM, United States
- ⁶⁷ Syracuse University, Syracuse, NY, United States
- ⁶⁸ Pontifícia Universidade Católica do Rio de Janeiro (PUC-Rio), Rio de Janeiro, Brazil, associated to ³
- ⁶⁹ School of Physics and Electronics, Hunan University, Changsha City, China, associated to ⁸
- ⁷⁰ Guangdong Provincial Key Laboratory of Nuclear Science, Guangdong-Hong Kong Joint Laboratory of Quantum Matter, Institute of Quantum Matter, South China Normal University, Guangzhou, China, associated to ⁴
- ⁷¹ Lanzhou University, Lanzhou, China, associated to ⁵
- ⁷² School of Physics and Technology, Wuhan University, Wuhan, China, associated to ⁴
- ⁷³ Departamento de Física, Universidad Nacional de Colombia, Bogota, Colombia, associated to ¹⁵
- ⁷⁴ Ruhr Universitaet Bochum, Fakultae f. Physik und Astronomie, Bochum, Germany, associated to ¹⁸
- ⁷⁵ Eotvos Lorand University, Budapest, Hungary, associated to ⁴⁷
- ⁷⁶ Van Swinderen Institute, University of Groningen, Groningen, Netherlands, associated to ³⁶
- ⁷⁷ Universiteit Maastricht, Maastricht, Netherlands, associated to ³⁶
- ⁷⁸ Tadeusz Kosciuszko Cracow University of Technology, Cracow, Poland, associated to ³⁹
- ⁷⁹ Universidade da Coruña, A Coruna, Spain, associated to ⁴³
- ⁸⁰ Department of Physics and Astronomy, Uppsala University, Uppsala, Sweden, associated to ⁵⁸
- ⁸¹ University of Michigan, Ann Arbor, MI, United States, associated to ⁶⁷

⁸²*Departement de Physique Nucleaire (SPhN), Gif-Sur-Yvette, France*

^a*Universidade de Brasília, Brasília, Brazil*

^b*Centro Federal de Educação Tecnológica Celso Suckow da Fonseca, Rio De Janeiro, Brazil*

^c*Hangzhou Institute for Advanced Study, UCAS, Hangzhou, China*

^d*School of Physics and Electronics, Henan University, Kaifeng, China*

^e*LIP6, Sorbonne Université, Paris, France*

^f*Universidad Nacional Autónoma de Honduras, Tegucigalpa, Honduras*

^g*Università di Bari, Bari, Italy*

^h*Università degli studi di Bergamo, Bergamo, Italy*

ⁱ*Università di Bologna, Bologna, Italy*

^j*Università di Cagliari, Cagliari, Italy*

^k*Università di Ferrara, Ferrara, Italy*

^l*Università di Firenze, Firenze, Italy*

^m*Università di Genova, Genova, Italy*

ⁿ*Università degli Studi di Milano, Milano, Italy*

^o*Università degli Studi di Milano-Bicocca, Milano, Italy*

^p*Università di Padova, Padova, Italy*

^q*Università di Perugia, Perugia, Italy*

^r*Scuola Normale Superiore, Pisa, Italy*

^s*Università di Pisa, Pisa, Italy*

^t*Università della Basilicata, Potenza, Italy*

^u*Università di Roma Tor Vergata, Roma, Italy*

^v*Università di Siena, Siena, Italy*

^w*Università di Urbino, Urbino, Italy*

^x*Universidad de Alcalá, Alcalá de Henares, Spain*

^y*Facultad de Ciencias Físicas, Madrid, Spain*

^z*Department of Physics/Division of Particle Physics, Lund, Sweden*

[†]*Deceased*